Human Movement Science 63 (2019) 209–230

Contents lists available at ScienceDirect

Human Movement Science

journal homepage: www.elsevier.com/locate/humov

Motion planning strategies in human control of non-rigid objects with internal degrees of freedom

Mikhail Svinin[a,*], Igor Goncharenko[a], Victor Kryssanov[a], Evgeni Magid[b]

[a] College of Information Science and Engineering, Ritsumeikan University, 1-1-1 Nojihigashi, Kusatsu, Shiga 525-8577, Japan
[b] Department of Intelligent Robotics, Kazan Federal University, Kremlyovskaya Str. 35, Kazan 420008, Russian Federation

ARTICLE INFO

Keywords:
Reaching movements
Dynamic environment
Flexible object
Trajectory planning
Optimization models

ABSTRACT

The paper deals with modeling of human-like reaching movements in dynamic environments. A simple but not trivial example of reaching in a dynamic environment is the rest-to-rest manipulation of a multi-mass flexible object with the elimination of residual vibrations. Two approaches to the prediction of reaching movements are formulated in position and force actuation settings. In the first approach, either the position of the hand or the hand force is specified by the lowest order polynomial satisfying the boundary conditions of the reaching task. The second approach is based on the minimization of either the hand jerk or the hand force-change, with taking into account the dynamics of the flexible object. To verify the resulting four mathematical models, an experiment on the manipulation of a ten-masses flexible object of low stiffness is conducted. The experimental results show that the second approach gives a significantly better prediction of human movements, with the minimum hand force-change model having a slight but consistent edge over the minimum hand jerk one.

1. Introduction

When humans make point-to-point movements in free space, there is, in principle, an infinite choice of trajectories. However, many studies have shown that the hand trajectories in such movements are highly stereotypical under a large variety of experimental conditions. In particular, human subjects tend to produce trajectories with the following invariant features. First, hand paths in point-to-point movements appear to be straight and smooth. Second, for relatively fast movements the velocity profile of the hand trajectory comes out bell-shaped (Morasso, 1981; Abend, Bizzi, & Morasso, 1982). These invariant features may correlate with the internal representation of the movements in the central nervous system (CNS), presuming that the hand trajectories are planned in extracorporeal space (Bernstein, 1967). Also, they can serve as a standard for judging whether a reaching movement is human-like or not. The latter is of not only theoretical but also practical interest, especially in the emergent field of collaborative robotics. As was demonstrated by Maurice, Huber, Hogan, and Sternad (2018), the physical human-robot interaction was facilitated when the invariant features of human movements, captured by the empirical *two-thirds power law* (Lacquaniti, Terzuolo, & Viviani, 1983), were taken into account in the robot control system.

Modeling of human-like reaching movements is a very important research problem in neurophysiology, computational neuroscience, and robotics (Pollick, Hale, & Tzoneva-Hadjigeorgieva, 2005; Amirabdollahian, Loureiro, & Harwin, 2002). From the viewpoint of control theory the problem can be approached from two directions: one focuses on the open-loop feedforward control

* Corresponding author.
E-mail addresses: svinin@fc.ritsumei.ac.jp (M. Svinin), igor@fc.ritsumei.ac.jp (I. Goncharenko), kvvictor@is.ritsumei.ac.jp (V. Kryssanov), magid@it.kfu.ru (E. Magid).

https://doi.org/10.1016/j.humov.2018.12.004
Received 15 August 2018; Received in revised form 9 December 2018; Accepted 13 December 2018
Available online 28 December 2018
0167-9457/

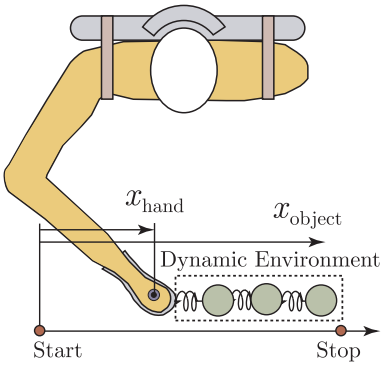

Fig. 1. Reaching movement in the manipulation of flexible objects.

(Kawato, 1999; Flash, Hogan, & Richardson, 2003), and another is based on the feedback control (Hoff & Arbib, 1993; Tsuji, Tanaka, Morasso, Sanguineti, & Kaneko, 2002; Arimoto, Sekimoto, Hashiguchi, & Ozawa, 2005). In this paper we will deal with the feedforward control of reaching movements. The reasoning behind the use of this control scheme is that in fast reaching movements the effective use of feedback is nearly impossible due to the delays in neural circuits and muscle activation.

The feedforward control is often modeled via optimization theory. In this approach, the trajectory of the human hand is predicted by minimizing an integral performance index subject to boundary conditions imposed on start and end points. It is well established that for the unconstrained reaching movements the trajectory of human hand can be predicted with reasonable accuracy by the minimum hand jerk (MHJ) criterion (Flash & Hogan, 1985). Another popular model is based on the minimum joint torque change criterion (Uno, Kawato, & Suzuki, 1989).

While the optimization models in motor control are not fully accurate, they can capture the invariant features of unconstrained reaching movements, in particular the bell-shaped velocity profile, reasonably well. However, this can be done by a variety of functional relations (Plamondon, Alimi, Yergeau, & Leclere, 1993) not necessarily based on the optimization models. In this connection, the design of critical tests for reaching tasks, featuring not only a single-peaked bell shape but more complex shapes of the hand velocity profiles, is a very important research problem (Engelbrecht, 2001). To approach this problem, one can "place" the human hand in an artificially created dynamic environment.

An example of reaching in a dynamic environment (see Fig. 1) is the rest-to-rest manipulation of a linear chain of flexible objects with suppression of structural vibrations at the end of movement. Despite the seeming simplicity, this task requires a certain skill that must be acquired through practicing. The difficulty stems from the fact that the system under control is under-actuated. It has multiple degrees of freedom controlled by a single input. An interesting feature of this task, first observed by Dingwell, Mah, and Mussa-Ivaldi (2004) in experiments with one-mass flexible object, is that under certain conditions the human controls the object in a very non-trivial way, keeping two distinct phases in the hand velocity profile.

Considering this manipulation task from the control engineering point of view, one can find different strategies to generate rest-to-rest motion commands that eliminate residual vibrations (Smith, 1957; Aspinwall, 1990; Singer & Seering, 1990; Karnopp, Fisher, & Yoon, 1992; Meckl & Kinceler, 1994; Chan & Stelson, 1995). Perhaps the simplest open-loop control strategy is to specify the motion of the most distal link of the flexible object by the lowest order polynomial (LOP) satisfying the boundary conditions (Piazzi et al., 2000; Lévine & Nguyen, 2003; Sira-Ramírez & Agrawal, 2004). This control strategy has been successfully applied to modeling of reaching movements in the manipulation of one flexible object (Dingwell et al., 2004). However, this strategy does not capture well the velocity profiles of reaching movements in the case of multi-mass flexible objects, and is less consistent in comparison with the MHJ model (Svinin, Goncharenko, Luo, & Hosoe, 2006).

Another possible strategy to plan the reaching movement with the flexible object is to specify by the LOP the motion of not the most distal link but the foremost link that is the hand. It is well known that minimization of the hand jerk for reaching movements in free space is mathematically equivalent to matching the boundary conditions imposed on the hand position, velocity and acceleration by the LOP (Flash & Hogan, 1985). However, as will be shown in this paper, the LOP strategy based on simple matching of the boundary conditions and the strategy based on the minimization of the control effort (the hand jerk) are not mathematically equivalent for reaching movements in dynamic environments. It is, therefore, of interest to compare these strategies of the hand trajectory formation and examine how well they capture the patterns of human movements.

It should be noted that the above specified two movement strategies can be formulated in kinematic (as discussed above) or dynamic (when the inertia of the human hand is not ignored) settings, resulting into four computational models. The dynamic counterpart of the MHJ model is the minimum hand force-change (MHFC) model. Likewise, the dynamic equivalent of the kinematic LOP model is the LOP specification of the hand driving force. It is interesting to note that the latter model can be linked to the definition of natural motion in analytical mechanics (Morita & Ohtsuka, 2006; Morita, 2012) and to the Gauss principle of least constraint for the control of mechanical systems (Soltakhanov, Yushkov, & Zeghda, 2009; Zegzhda, Shatrov, & Yushkov, 2016). In this connection, it is worthwhile to investigate how this formal way of the construction of natural motion works in the context of natural human movements in comparison with the MHJ and MHFC models. This constitutes the main goal of this paper.

For the experimental verification of the above-stated models, we select a flexible object with large enough number of masses

because the difference between theoretical predictions may correlate with the number of degrees of freedom of the object (Svinin et al., 2006). It should be noted that in (Svinin et al., 2006) the authors experimented with relatively stiff object and observed single-peaked bell-shaped profiles of the hand velocity. To obtain the experimental data, we test the manipulation of a flexible object of a low stiffness. The data collected reveal the appearance of two sharply distinct phases of motion. Our analysis of the experimental data confirms that the minimum control effort-based strategy represented by the MHJ and MHFC models, which, compare to the simple matching of the boundary conditions, reflects the notion of optimality, provides a better and quite satisfactory fit to the experimental data.

The rest of the paper is organized as follows. In Section 2, we formalize a mathematical description of the flexible object and the boundary conditions for the reaching task. In Section 3 we establish the mathematical structure of four theoretical models, the kinematic and dynamic versions of the LOP-based movement strategy, and the kinematic and dynamic versions (MHJ and MHFC models) of the minimum control effort-based strategy. Analytical solutions provided by these models are tested against experimental data in Section 4 which also describes the experimental setup and the protocol of collecting the data. Finally, the study is discussed and conclusions are summarized in Section 5.

2. Model of the dynamic environment

In this section we formalize reaching movements in a dynamic environment that is modeled as a multi-mass flexible object. For the sake of simplicity, we deal with a one-dimensional model of human movements. In this model the configuration dependance of the human arm is ignored and the motion is considered at the hand level. First, we set up the dynamic model of the object, then define a reaching task, and formulate its boundary conditions.

2.1. System dynamics

Assume that the object to be manipulated is composed of n beads of mass m connected by n springs of stiffness coefficient k as shown in Fig. 2. For the uniform mass and stiffness distribution, the dynamic equations can be written down as follows

$$m_0\ddot{x}_0 + k(x_0 - x_1) = f, \tag{1}$$

$$m\ddot{x}_s + k(x_s - x_{s-1}) + k(x_s - x_{s+1}) = 0, \tag{2}$$

$$m\ddot{x}_n + k(x_n - x_{n-1}) = 0, \tag{3}$$

where x_s, $s = 1, \ldots, n$, are the positions of the beads, x_0 stands for the position of the hand, m_0 is the hand mass, and f is the driving force.

For establishing trajectory formation models it is convenient to represent the system's dynamics in terms of the object end position x_n. The dynamics of the flexible object (2, 3) can be rearranged as

$$x_{s-1} = \frac{1}{\omega^2}\ddot{x}_s + 2x_s - x_{s+1}, \quad s = 1, \ldots, n-1, \tag{4}$$

$$x_{n-1} = \frac{1}{\omega^2}\ddot{x}_n + x_n, \tag{5}$$

where $\omega = \sqrt{k/m}$, and the hand position x_0 can be expressed in terms of the position of the last bead x_n and its derivatives. By solving Eqs. (4) and (5) recurrently for $s = n-1, n-2, \ldots, 1$, one obtains (Svinin et al., 2006):

$$\sum_{l=0}^{s} \frac{C_{s+l}^{s-l}}{\omega^{2l}} x_n^{(2l)}(t) = x_{n-s}(t), \tag{6}$$

where $C_p^q = p!/(q!(p-q)!)$ denotes the binomial coefficients, and $x_n^{(2l)}$ stands for the $2l$-th time derivative of the n-th coordinate.

By setting $s = n$ in (6), one converts the system of n differential equations of the 2nd order (2, 3) to one differential equation of the $2n$-th order

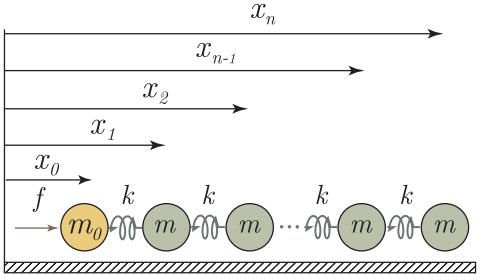

Fig. 2. Multi-mass flexible object driven by the hand.

$$\sum_{l=0}^{n} \frac{C_{n+l}^{n-l}}{\omega^{2l}} x_n^{(2l)}(t) = x_0(t), \tag{7}$$

which describes the dynamics of flexible object under kinematic actuation by the hand position x_0.

By combining (7), (1), and (6) taken for $s = n - 1$, one converts the system of $n + 1$ differential equations of the 2nd order (1)–(3) to one differential equation of the $2(n + 1)$-th order

$$\sum_{l=0}^{n} \frac{C_{n+l}^{n-l}}{\omega^{2l}} \left\{ m_0 x_n^{(2l+2)}(t) + \frac{2lk}{n+l} x_n^{(2l)}(t) \right\} = f(t), \tag{8}$$

which describes the dynamics of the combined system, composed of the hand and the flexible object, driven by the hand force f.

2.2. Reaching task and the boundary conditions

Assume that a human subject makes a reaching movement of length L and time T and stops at the target point the hand and all the beads of the object without excitation of oscillations. In the engineering terminology, the subject generates a rest-to-rest motion command that eliminates residual vibrations.

Without loss of generality we assume that the subject transports all the beads from the initial state

$$x_s(0) = 0,\ \dot{x}_s(0) = 0,\ \ s = 1,\ ...,n, \tag{9}$$

to the final state

$$x_s(T) = L,\ \dot{x}_s(T) = 0,\ \ s = 1,\ ...,n. \tag{10}$$

Assuming that the hand is at rest in the beginning and in the end of the reaching movement, one has

$$x_0(0) = 0,\ \ \dot{x}_0(0) = 0,\ \ \ddot{x}_0(0) = 0, \tag{11}$$

$$x_0(T) = L,\ \ \dot{x}_0(T) = 0,\ \ \ddot{x}_0(T) = 0. \tag{12}$$

In what follows, we will derive trajectory formation models in terms of the object end position and for this purpose we need to formulate the boundary conditions for $x_n(t)$ and its higher derivatives. They can be obtained from the boundary conditions (9) and (10) and (11) and (12). Differentiating Eqs. (4) and (5) sequentially, s-th equation 2 s times, and considering them at $t = 0$ and $t = T$, one obtains

$$x_s^{(2)}(0) = x_s^{(3)}(0) = ...=x_s^{(2s+2)}(0) = 0, \tag{13}$$

$$x_s^{(2)}(T) = x_s^{(3)}(T) = ...=x_s^{(2s+2)}(T) = 0. \tag{14}$$

Combining (9) and (10) and (13) and (14) for $i = n$, one establishes the boundary conditions for the object end position:

$$x_n(0) = 0,\ \dot{x}_n(0) = ...=x_n^{(2n+2)}(0) = 0, \tag{15}$$

$$x_n(T) = L,\ \dot{x}_n(T) = ...=x_n^{(2n+2)}(T) = 0. \tag{16}$$

In total, we have $2(2n + 3)$ boundary conditions.

3. Motion planning strategies

In this section, we outline two motion planning strategies for the reaching task under consideration, the LOP model for the control input and the model based on the minimization of squared control effort integrated over the movement time.

For each of the strategies we will consider two types of actuation, position-based and force-based. For the position-based actuation, the actuator dynamics (i.e., the hand dynamics (1)) do not play an independent role in establishing motion trajectories, and are not included in model (7). It is thus assumed that the human arm, controlled by the CNS, is an ideal actuator driving the hand in the task space. Under such an assumption inertial properties of the arm are not taken into consideration (Flash & Hogan, 1985).

For the force-based actuation the hand dynamics (1) and the hand mass are included in model (8). It is thus assumed that the CNS does take into account inertial properties of the arm (Uno et al., 1989). The hand driving force is directly involved in defining motion trajectories while in the position-based actuation it is estimated after establishing the motion trajectories.

3.1. LOP strategy: position-based actuation

The dynamics of the last bead in (7) are actuated by the hand position x_0. One way to plan reaching movements for the task defined in Section 2.2 is to specify the motion of the hand, $x_0(t)$, in the form of the LOP satisfying the boundary conditions (15) and (16). For $x_0(t) = 0$ Eq. (7) has $2n$ integration constants. The total number of the boundary conditions (15, 16) is $2(2n + 3)$. Therefore, the differential equation for the lowest order polynomial control input $x_0(t)$ must have the order $2(2n + 3) - 2n = 2n + 6$. Thus, one has $x_0^{(2n+6)}(t) = 0$ and therefore

$$x_0(t) = \sum_{i=0}^{2n+5} a_i t^i, \tag{17}$$

where a_i are unknown constant coefficients.

By differentiating (7) $2n + 6$ times, one obtains the following linear differential equation

$$\sum_{s=0}^{n} \frac{C_{n+s}^{n-s}}{\omega^{2s}} x_n^{(2(n+s)+6)}(t) = 0. \tag{18}$$

Its characteristic equation,

$$\lambda^{2n+6}\left(\sum_{s=0}^{n} \frac{C_{n+s}^{n-s}}{\omega^{2s}}\lambda^{2s}\right) = 0, \tag{19}$$

has $2n + 6$ zero roots and n pairs of imaginary roots $\lambda = \pm\imath p_s$, where p_s, $s = 1, 2, ..., n$, are the natural frequencies of the flexible object defined by Eq. (48) in Appendix A.1. The trajectory of the last bead is therefore defined as

$$x_n(t) = \sum_{i=0}^{2n+5} \alpha_i t^i + \sum_{i=1}^{n} \beta_i \sin\left(p_i t + \gamma_i\right), \tag{20}$$

where the $4n + 6$ coefficients α_i, β_i, γ_i are calculated from the $4n + 6$ boundary conditions (15, 16). The substitution of (20) into (7) results in a polynomial form (see Appendix B.1), from which one can find the coefficients a_i in (17).

3.2. LOP strategy: force-based actuation

This strategy is closely related to the approach for generation of human-like reaching movements based on the modified Hamilton principle and on the definition of natural systems adopted in analytical mechanics (Morita & Ohtsuka, 2006; Morita, 2012). For the convenience of the reader we summarize this approach in Appendix C. Note that the natural reaching movement in (Morita & Ohtsuka, 2006; Morita, 2012) is defined for the fully actuated systems. However, the same reasoning—setting the control input in the LOP form—can be applied for underactuated systems as well.

The dynamics of the last bead in (8) are actuated by the hand force f. For $f(t) = 0$ Eq. (8) has $2(n + 1)$ integration constants. The total number of the boundary conditions (15) and (16) is $2(2n + 3)$. Therefore, the differential equation for the lowest order polynomial control input $x_0(t)$ must have the order $2(2n + 3) - 2(n + 1) = 2n + 4$. Thus, one has $f^{(2n+4)}(t) = 0$ and therefore

$$f(t) = \sum_{i=0}^{2n+3} f_i t^i, \tag{21}$$

where f_i are unknown constant coefficients.

By differentiating (8) $2n + 4$ times, one obtains the following linear differential equation:

$$\sum_{l=0}^{n} \frac{C_{n+l}^{n-l}}{\omega^{2l}}\left\{x_n^{(2(n+l)+6)}(t) + \frac{2l\mu\omega^2}{n+l} x_n^{(2(n+l)+4)}(t)\right\} = 0, \tag{22}$$

where the mass ratio $\mu = m/m_0$. The characteristic equation corresponding to (22) can be represented as

$$\lambda^{2n+6}\left(\sum_{s=0}^{n} \frac{C_{n+s}^{n-s}}{\omega^{2s}}\left\{\lambda^{2s} + \frac{2s\mu\omega^2}{n+s}\lambda^{2(s-1)}\right\}\right) = 0. \tag{23}$$

This equation has $2n + 6$ zero roots and n pairs of imaginary roots $\lambda = \pm\imath\tilde{p}_s$, where $\tilde{p}_s$, $s = 1, 2, ..., n$, are the natural frequencies of the combined (hand & flexible object) system defined by Eq. (54) in Appendix A.2. The trajectory of the last bead is therefore defined as

$$x_n(t) = \sum_{i=0}^{2n+5} \alpha_i t^i + \sum_{i=1}^{n} \beta_i \sin\left(\tilde{p}_i t + \gamma_i\right), \tag{24}$$

where the $4n + 6$ coefficients α_i, β_i, γ_i are defined from the $4n + 6$ boundary conditions (15, 16). Since the natural frequencies $\tilde{p}_i$ differ from p_i defined from (48), the structure of the hand trajectory x_0 mimics that of x_n:

$$x_0(t) = \sum_{i=0}^{2n+5} a_i t^i + \sum_{i=1}^{n} b_i \sin\left(\tilde{p}_i t + c_i\right), \tag{25}$$

where coefficients a_i, b_i, c_i are obtained by plugging (24) into (7).

3.3. Minimum control effort strategy: the MHJ model

Consider now the MHJ model in which the system trajectories are defined by minimizing the criterion

$$J = \frac{1}{2}\int_0^T \left(\frac{\mathrm{d}^3 x_0}{\mathrm{d}t^3}\right)^2 \mathrm{d}t. \tag{26}$$

Differentiating the hand position (7) three times and substituting the result into (26), one obtains

$$J = \frac{1}{2}\int_0^T \left(\sum_{l=0}^{n} \frac{C_{n+l}^{n-l}}{\omega^{2l}} x_n^{(2l+3)}\right)^2 \mathrm{d}t. \tag{27}$$

Denote by $\mathscr{L}$ the integrand of criterion (27). The trajectory $x_n(t)$ minimizing J under the boundary conditions (15) and (16) must satisfy the Euler–Lagrange equation

$$\sum_{k=0}^{2n+3} (-1)^k \frac{\mathrm{d}^{(k)}}{\mathrm{d}t^{(k)}}\left\{\frac{\partial \mathscr{L}}{\partial x_n^{(k)}}\right\} = 0. \tag{28}$$

For the given structure of $\mathscr{L}$, (28) reduces to the following linear differential equation:

$$\sum_{s=0}^{n}\sum_{l=0}^{n} \frac{C_{n+s}^{n-s} C_{n+l}^{n-l}}{\omega^{2s}\omega^{2l}} x_n^{(2\{l+s+3\})} = 0. \tag{29}$$

It can be shown that the characteristic equation corresponding to (29) is given by

$$\lambda^6\left(\sum_{s=0}^{n} \frac{C_{n+s}^{n-s}}{\omega^{2s}}\lambda^{2s}\right)^2 = 0. \tag{30}$$

This equation has 6 zero roots and $2n$ pairs of imaginary roots $\lambda = \pm\imath p_s$, where p_s, $s = 1, 2, \ldots, n$, are the natural frequencies of the flexible object defined by (48). The optimal trajectory of the last bead is therefore defined as

$$x_n(t) = \sum_{i=0}^{5} \alpha_i t^i + \sum_{i=1}^{n} \beta_i \sin\left(p_i t + \gamma_i\right) + t\,\delta_i \sin\left(p_i t + \varepsilon_i\right), \tag{31}$$

where constant coefficients α_i, β_i, γ_i, δ_i, ε_i are found from the boundary conditions (15) and (16).

To find the hand trajectory $x_0(t)$, one takes the even derivatives of (31) and substitute them into (7). As shown in Appendix B.2, the secular terms featured in the second sum of (31) then disappear, and the structure of the hand trajectory is defined as

$$x_0(t) = \sum_{i=0}^{5} a_i t^i + \sum_{i=1}^{n} b_i \sin\left(p_i t + c_i\right), \tag{32}$$

where a_i, b_i, c_i are constant coefficients. Thus, the optimal hand trajectory is composed of a 5-th order polynomial (as in the classical MHJ model of reaching movements in free space (Flash & Hogan, 1985)) and additional trigonometric terms.

3.4. Minimum control effort strategy: the MHFC model

In the MHFC model the system trajectories are defined by minimizing the criterion

$$J = \frac{1}{2}\int_0^T \left(\frac{\mathrm{d}f}{\mathrm{d}t}\right)^2 \mathrm{d}t. \tag{33}$$

Differentiating the hand force (8) and substituting the result into (33), one obtains

$$J = \frac{m_0^2}{2}\int_0^T \left(\sum_{l=0}^{n} \frac{C_{n+l}^{n-l}}{\omega^{2l}}\left\{x_n^{(2l+3)} + \frac{2l\mu\omega^2}{n+l} x_n^{(2l+1)}\right\}\right)^2 \mathrm{d}t. \tag{34}$$

Denote by $\mathscr{L}$ the integrand of criterion (34). The trajectory $x_n(t)$ minimizing criterion (34) under the boundary conditions (15, 16) must satisfy the Euler–Lagrange Eq. (28) which, for the given structure of $\mathscr{L}$, reduces to the following linear differential equation:

$$\sum_{s=0}^{n}\sum_{l=0}^{n} \frac{C_{n+s}^{n-s} C_{n+l}^{n-l}}{\omega^{2s}\omega^{2l}}\left\{x_n^{(2\{l+s+3\})} + \frac{2(l+s)\mu\omega^2}{n+l+s} x_n^{(2\{l+s+1\})}\right\} = 0. \tag{35}$$

The characteristic equation corresponding to (35) can be represented as

$$\lambda^6\left(\sum_{s=0}^{n} \frac{C_{n+s}^{n-s}}{\omega^{2s}}\left\{\lambda^{2s} + \frac{2s\mu\omega^2}{n+s}\lambda^{2(s-1)}\right\}\right)^2 = 0. \tag{36}$$

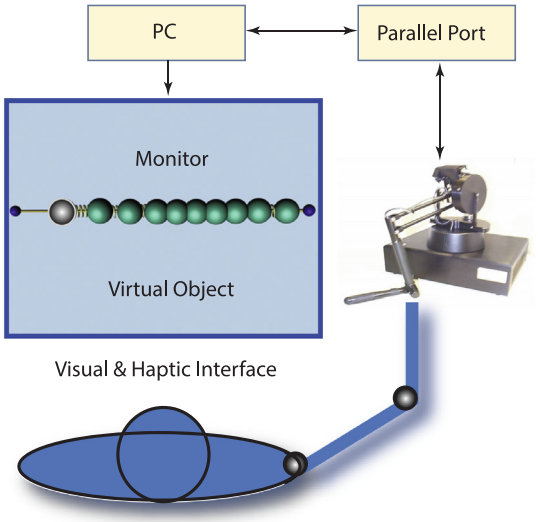

Fig. 3. Experimental setup.

This equation has 6 zero roots and $2n$ pairs of imaginary roots $\lambda = \pm\imath\, p_s^*$, where p_s^*, $s = 1, 2, \ldots, n$, are the natural frequencies of the combined (hand & flexible object) system. The optimal trajectory of the last bead is therefore defined as

$$x_n(t) = \sum_{i=0}^{5} \alpha_i t^i + \sum_{i=1}^{n} \beta_i \sin\left(p_i^* t + \gamma_i\right) + t\,\delta_i \sin\left(p_i^* t + \varepsilon_i\right), \tag{37}$$

where the constant coefficients α_i, β_i, γ_i, δ_i, ε_i are found from the boundary conditions (15) and (16). The optimal hand trajectory is then obtained upon substitution of (37) into (7), which results in

$$x_0(t) = \sum_{i=0}^{5} a_i t^i + \sum_{i=1}^{n} b_i \sin\left(p_i^* t + c_i\right) + t d_i \sin\left(p_i^* t + e_i\right), \tag{38}$$

where a_i, b_i, c_i are constant coefficients. Note that the obtained expression for the hand trajectory differs structurally from the one developed for the MHJ model.

4. Experiment

4.1. Experimental setup

To analyze velocity profiles of reaching movements with multi-mass objects, an experiment was conducted. In the experimental setup (see Fig. 3), an impedance-type haptic device (PHANToM Premium 151A/3DOF by SensAble Technologies) was used to generate real-time forces (maximum exertable force 8.5N). The haptic device was connected to a computer (Dell, 3.0 GHz) through a PCI interface.

Five naïve self-proclaimed, right-handed subjects (males, aged between 25 and 35 years old) participated in the experiments. All subjects were healthy, and gave informed consent. All procedures performed in the experiments were in accordance with the ethical standards of the institutional research committee and with the 1964 Helsinki declaration and its later amendments.

The subjects were instructed to move a multi-mass virtual flexible object, with the first mass (shown gray in Fig. 3) "connected" to the human hand by the haptic feedback generated by the PHANToM motors at a 1 kHz sampling frequency. The hand & object system was at rest at the start point. Before starting movements, the subject positioned the PHANToM pointer to the first bead and "connected" it to the hand (proxy point) by pressing a button on the computer keyboard. When recording the motion data, the subject pressed another button by the left hand and, at the same time, initiated the movement by the right hand.

The subjects were requested to move the flexible object in a single reaching movement and stop the hand and all the beads at a target point. The subjects made these rest-to-rest movements along a line (in the direction from left to right) in the horizontal plane using the PHANToM stylus. The one-dimensional movements were implemented in software by setting a higher constraint force in the directions orthogonal to the movement line. This force was realized by introducing a virtual spring (stiffness coefficient 600N/m), acting in the lateral directions. The haptic force acting along the movement line was computed as $k(x_1 - x_0)$, where x_0 is the position of the proxy (human hand) on the movement line, and x_1 is the position of the first bead of the object.

The positions of the hand and the beads were displayed on the computer monitor, providing the subject with real-time visual feedback. The object dynamics were simulated by using the conventional 4th-order Runge–Kutta method with constant step

$h = 0.001$s, and the real-time haptic feedback was supplied to the subject through the PHANToM stylus at the same rate (1 kHz). The hand position was measured by the PHANToM hardware (optical encoders placed on the motors). The hand velocity (the estimate averaged over 100 samples (Çavuşoğlu, Feygin, & Tendick, 2002)) was computed by the standard I/O commands of the OpenHaptics software toolkit (Itkowitz, Handley, & Zhu, 2005).

4.2. Experimental protocol

As the reaching movements under consideration are quite different from what one experiences in daily life, the experiment was conducted in three days. On the preliminary day we conducted a general evaluation of the subject performance. The subjects familiarized themselves with the experimental setup, comprehended the reaching task, performed movement trials, and learned the unusual dynamic environment. The subjects were asked to produce reaching movements in a natural way, on their own pace, trading off the speed (as fast as possible but not impulsively) and the comfort (as comfortable as possible). This instruction was necessary to keep up with the common assumption of the CNS operating without undue stress, away from the limits of neuromuscular performance (Flash & Hogan, 1985).

It was communicated that it might not be possible to reach the target point with zero velocity (for the hand and all the beads) in a single reaching movement, and the subjects were not requested to suppress the post-movement residual vibrations. A movement trial was considered successful if the task was completed within certain position and velocity tolerances. The subject was given an audio feedback, generated by the computer, when a trial was successful. No data regarding the motion trajectories were recorded during the preliminary evaluation as the main purpose was to select such parameters of the movement task that would guarantee an acceptable success rate and facilitate the learning process.

Several configurations of the flexible object were tested in the preliminary experiments. Assuming that the difference between theoretical predictions may correlate with the number of degrees of freedom (Svinin et al., 2006), we selected the object with a large enough number of beads. To make the reaching task not too easy, the object was to be configured with a low enough total stiffness. At the same time, to be able to collect a sufficient number of successful trials, one could not afford having a too flexible object. As there is no systematic way (known to us) to balance the complexity of the reaching task with a reasonably acceptable success rate, the whole tuning process needed to be done by trials and errors.

In the course of the preliminary experiments, we selected a flexible object of the total mass 3 kg and the total stiffness 10 N/m. The number of beads was set as $n = 10$, which resulted in $m = 0.3$ kg and $k = 100$ N/m. For the subsequent analysis we selected the reaching task with the traveling distance $L = 0.2$ m and the movement time[1] $T = 2.35$s. When selecting the latter parameter, we were guided by the following, mostly intuitive but practical considerations. For a given reaching task, there is the lowest limit when a successful trial can be detected. Below this limit the movement is neither smooth (impulsive) nor comfortable. Setting the movement time close to this limit would require longer time to learn the reaching task. Large values of T, on the other hand, would make the reaching task more repeatable, but they were out of interest. Thus, the "right" values of T could be set by trading off the time duration and the expected success rate.

Initially, the value of T was set to 2.0 s (exhibiting very low success rate) and then gradually increased until the movement felt more or less repeatable. For $T = 2.35$ s, it was observed that in successful trials the subjects produced a somewhat common movement strategy (see Fig. 4) that can be qualitatively described as follows. In the beginning, the positions of all the beads coincide at the start point. During the first half of the movement, the first (driving) bead is ahead of the last (most distal) bead, with the distance between them being about 5cm. During the second half of the movement the configuration is reversed symmetrically—the driving bead comes behind the last one and, finally, all the beads reach the target point.

To verify the observed movement strategy with a quantitative analysis, the parameters of the reaching task were subjected to tolerances. The reaching time tolerance was set as $\Delta T = \pm 0.45$s. For each of the beads, the position and velocity tolerances to be satisfied at the start and end points were selected as $\Delta x = \pm 0.012$ m and $\Delta v = \pm 0.024$ m/s. For the hand, the start and end point position and velocity tolerances were set as $\Delta x = \pm 0.012$ m and $\Delta v = \pm 0.05$ m/s. A movement trial now was considered successful if the subject was able to complete the reaching task within the tolerances specified above.

Having selected the parameters of the reaching task, we conducted further experiments in two days. On the first day, the subjects performed the reaching task and completed 600 trials. The subjects were provided with an audio feedback generated by the computer when a trial was successful. In addition, to facilitate the perception of the task timing, a time bar was displayed on the computer monitor. The time bar (see Fig. 5) reflected undershooting, hitting the time window, and overshooting in the time domain in, respectively, blue, green, and red colors. The subjects were instructed to stop motion (and recording by pressing a keyboard button) once the time tolerance, indicated by the time bar, was violated.

The experiment was divided into two blocks. Upon completing the first 300 trials (1st block) the subjects rested for about 30 min and then produced another 300 trials (2nd block). The overall success rate achieved on the first day of the experiment is shown in Table 1. On the second day the experiment was repeated in the same order and the subjects produced another 600 trials. The data regarding the position and velocity of the hand and those of the simulated beads were collected for analysis. These data were recorded at the sampling frequency of 100 Hz sufficient to analyze human movements with an average reaction time of 200 ms.

Having completed the main set of trials in reaching movements, the subjects rested for about one hour and then were engaged in a completely different experiment where they simply followed a periodic force produced by the PHANToM device along the same line

[1] It was necessary to fix T because the theoretical models under verification (refer to Section 3) presume fixed movement time.

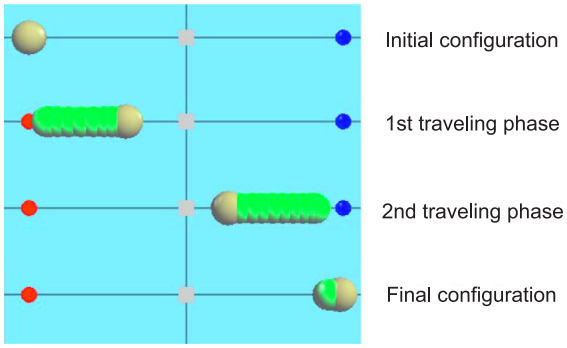

Fig. 4. A typical movement strategy observed in the preliminary trials.

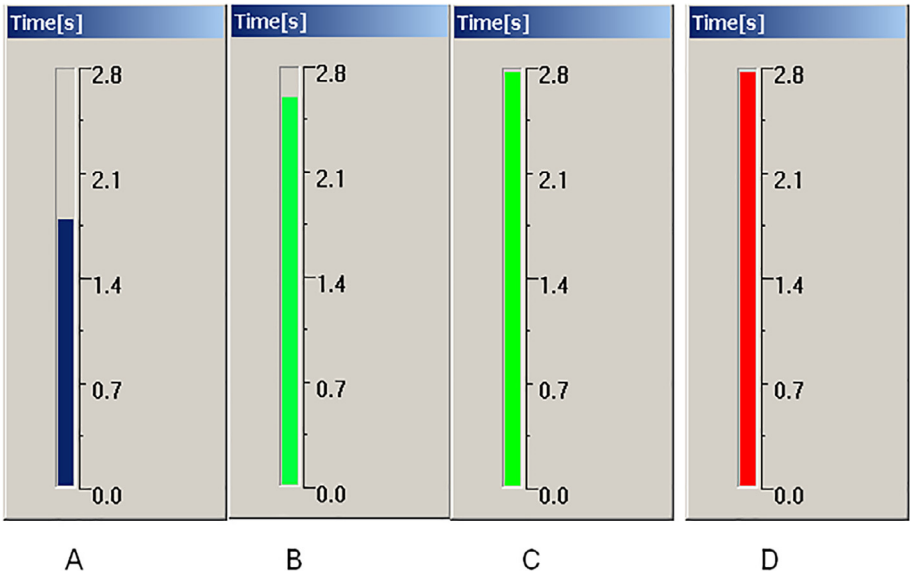

Fig. 5. The time bar: A–a trial is in process, not reaching the time tolerance window; B–a trial is within the time tolerance window; C–a trial is successfully completed; D–a trial is failed.

Table 1
Progress in motor training: number of successful trials and, in parentheses, the success rate [%].

Subject	Day 1	Day 2	Total
S1	54 (9.00)	68 (11.33)	122 (10.17)
S2	68 (11.33)	94 (15.67)	162 (13.50)
S3	84 (14.00)	89 (14.83)	173 (14.41)
S4	80 (13.33)	96 (16.00)	176 (14.67)
S5	100 (16.67)	119 (19.83)	219 (18.25)

of constraint as in the reaching movements. The purpose of this additional experiment was to identify the effective hand mass m_0 for the use in the MHFC and the dynamic LOP models. Details of this experiment are described in Appendix D, and results are reported in Table 5 of Appendix D.

4.3. Experimental results: learning history

The numbers of successful trials achieved by each subject and the corresponding success rates are listed in Table 1. It is interesting to note that in the second day of the experiment the success rate slightly increased for all the subjects. This may be linked to the recovery of movement skills (for the learnt reaching task) and the increase of the motor memory. It is partially reflected in the learning histories presented in left column of Fig. 6, where the successful trials are marked by black vertical lines.

The resulting success rates are still far from perfect after two days of practicing, that can be attributed to the complexity of the reaching task requiring a high-level of coordination skills. One may speculate that more training would be necessary to achieve a

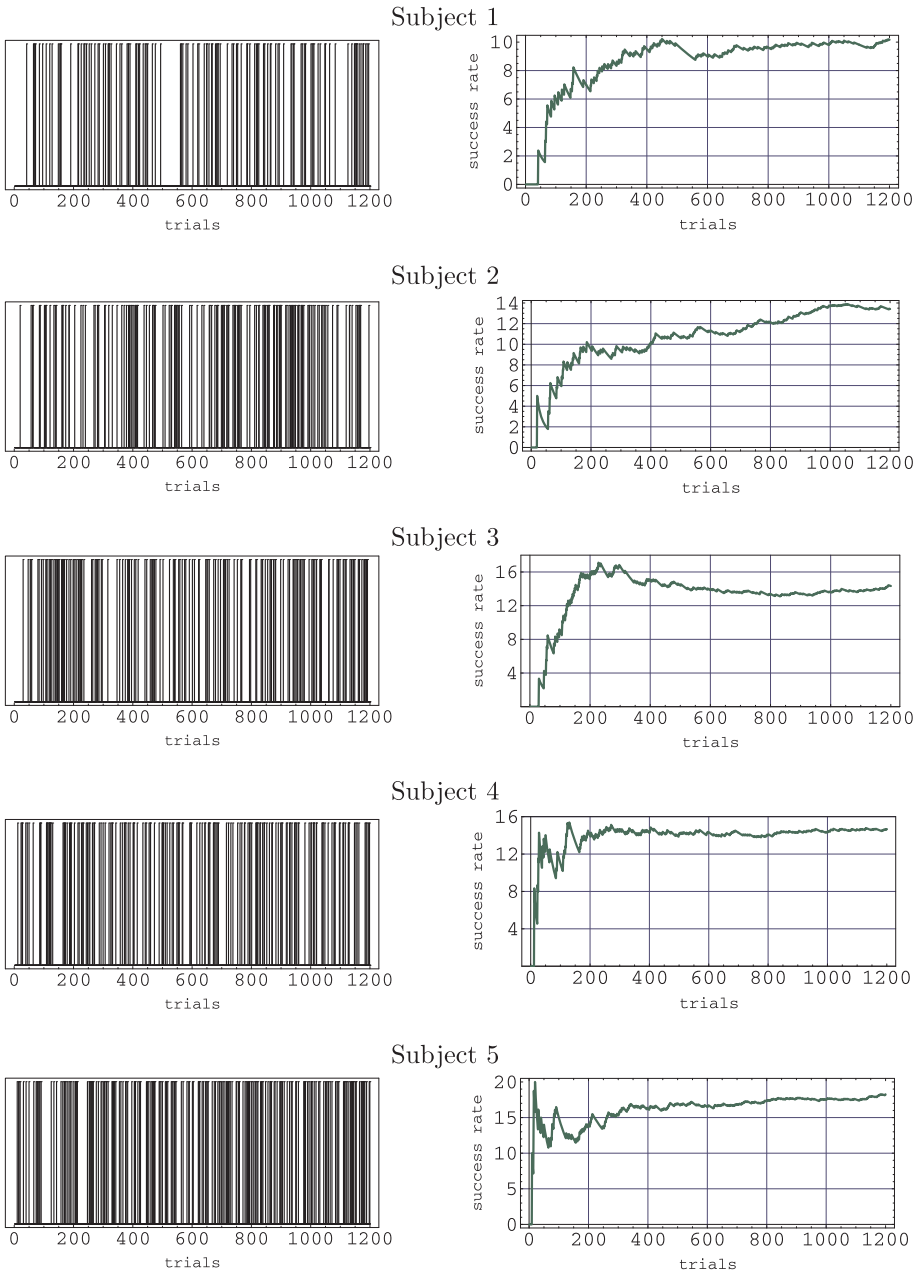

Fig. 6. Learning histories (left): black vertical lines correspond to successful trials. Evolution of the success rate (in percentages) as a function of the number of trials (right). (For interpretation of the references to colour in this figure legend, the reader is referred to the web version of this article.)

higher success rate for such a complex movement. However, the dynamics of the success rate shown in right column of Fig. 6 indicate that after certain numbers of trials the success rate appears to reach a plateau. The correlation between practice and performance on the learning curves is certainly not linear but rather exponential. This pattern holds for all the subjects and is, in a reasonable approximation, compatible with the classic power low of practice (Newell & Rosenbloom, 1981).

The apparent stabilization of the success rates at relatively low values may highlight the limits of the motor skills that can be developed within the adopted experimental protocol. It should be noted that the protocol is based on the unsupervised learning paradigm where the subject is supposed to increase his motor skill based on his own experience, reinforcing it upon producing successful trials. To increase the success rates, one might need to employ supervised learning. However, this consideration remains speculative, and is out of the scope of this study as no trainer was available for coaching and teaching the subjects.

Table 2
Movement time [s].

Subject	Avg.	Min.	Max.	SD
S1	2.258	1.972	2.723	0.215
S2	2.280	2.011	2.748	0.206
S3	2.261	1.959	2.742	0.213
S4	2.260	1.962	2.751	0.225
S5	2.237	1.957	2.753	0.189

4.4. Experimental results: trajectory profiles

Despite the relatively low success rates, the total number of successful trials, ranging across the subjects from 122 to 219, is not small and is, in our opinion, acceptable for conducting a comparative analysis of the experimental and theoretical motion profiles.

The average, minimum, and maximum times shown by the subjects in the successful trials are listed in Table 2. The table also provides the standard deviations (SD) from the averages. It should be noted that the fastest completion time (1.96 s) is very close to the lower bound admissible by the time tolerance. Since the time tolerance was relatively wide (about 20% of the time duration) and no subject hit successfully the lower limit of 1.90 s admitted by the tolerance, one can assert that the subjects did move on their own paces as instructed, trading off the speed and the comfort. It is perhaps possible to produce faster reaching movements under the given experimental conditions. However, with a shorter movement time one would expect a slower learning rate (and a lower success rate), as the human control system would get closer to the limits of neuromuscular performance.

The position, velocity, and acceleration of the hand and the last bead of the object were analyzed. Note that the acceleration of the last bead was computed in the online simulation, while that of the hand was obtained in post processing by numerical differentiation of the hand velocity. Before differentiating, the hand velocity profiles were smoothed by the moving average filter (Smith, 2002), with the number of samples set to five, corresponding to 50 ms interval of averaging. A visual examination of the obtained experimental profiles revealed qualitatively similar motion patterns for all the subjects. In particular, the position profiles looks like a single sigmoid for the last bead of the flexible object and a double sigmoid for the hand. Correspondingly, the velocity profiles features a single bell shape for the last bead and two distinct bell shapes for the hand.

The data of the last ten successful trials of each subject were taken for the visual comparison with the theoretical predictions. To compare motions of different durations graphically, the experimental position, velocity, and acceleration profiles of the hand and the last bead of the object were time scaled (Morasso, 1981; Atkeson & Hollerbach, 1985; Garvin, Žefran, Henis, & Kumar, 1997) using the average time of all the successful trials for each subject. Experimental trajectory profiles of the hand and the last bead for a representative subject (Subject 3) are shown in Fig. 7. The mean values are plotted with dark green and contoured by the plus/minus SD tubes shown with the light green color.

The average values of the effective hand mass m_0 (refer to Table 5 of Appendix D) were used in computing the corresponding theoretical profiles. The predictions by the MHJ and MHFC models are shown in Fig. 7 with, respectively, the blue and red lines. The predictions by the kinematic and dynamic LOP models are shown with, respectively, the solid gray and dashed black lines. It is observed that, despite fundamental differences in the definitions, the two LOP models result in almost identical[2] predictions for the estimated hand masses and the selected parameters of the flexible object and the reaching task.

As can be seen from Fig. 7, all the theoretical models under consideration qualitatively capture the basic tendencies of human movements in the manipulation of the flexible object. In particular, the models predict the bell-shaped profiles for the velocity of the last bead of the object and the two-phased profiles for the hand velocity. Quantitatively, however, the collected experimental data are certainly in favor of the optimization-based models, as the LOP models produce considerable overshoot for velocities (0.1 m/s for the hand and 0.2 m/s for the last bead) and accelerations (0.35 m/s^2 for the hand and 0.5 m/s^2 for the last bead). Since the large deviations (amounting to almost 50%) in the predictions by the LOP models were observed for all subjects, the LOP models can be ruled out of further consideration.

4.5. Comparison of the MHJ and MHFC Models

To determine which of the remaining models, MHJ or MHFC, produces a better match, we computed the root-mean-square (RMS) estimates of the trajectory errors (deviations from the experimental data) for the both models. For the k-th successful trial this quantitative measure is defined as

$$\mathrm{RMS}_k = \sqrt{\frac{1}{N}\sum_{i=1}^{N}\{s_k(t_i) - s^*(t_i)\}^2}, \tag{39}$$

where N is the number of sampled data in the trial, s_k is the trajectory observed in the experiment, and s^* is the trajectory predicted by

[2] As verified by simulation, the difference between the kinematic and dynamic LOP models for the selected flexible object becomes more distinct when the mass of the hand is less than 0.25 kg

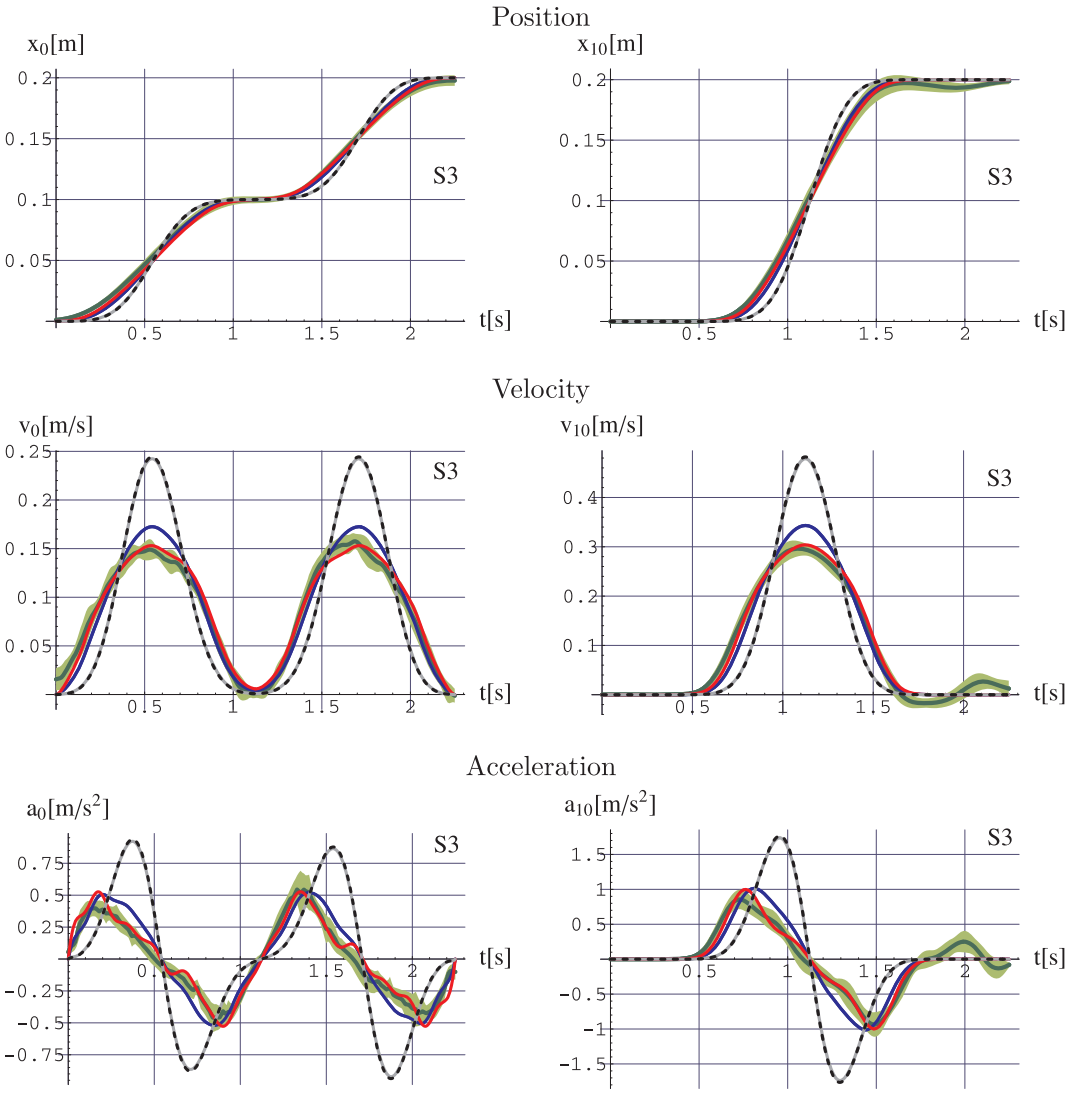

Fig. 7. Hand (left column) and the last bead (right column) position (1st row), velocity (2nd row) and acceleration (3rd row) profiles, predicted by the MHJ (blue), the MHFC (red), the kinematic LOP (gray), and the dynamic LOP (dashed black) models in comparison with experimental data: mean values, shown with the dark green lines, are contoured by ± SD band (light green). (For interpretation of the references to colour in this figure legend, the reader is referred to the web version of this article.)

the theoretical models. Here, *s* stands either for position, velocity, or acceleration. Note that the RMS deviations were calculated for the original (non-time-scaled) samples.

The RMS errors for the position, velocity, and accelerations of the hand and the last bead predicted by the MHJ and MHFC models are drawn for all subjects in the form of error bars (mean value plus/minus SD) in Fig. 8 with, respectively, blue and red colors. As expected, for the both models the position errors are substantially lower that the velocity ones, which in turn, are lower than the acceleration errors. It should also be noted that for both the models the errors for the last bead are larger than those for the hand. This is due to the sequential structure of the flexible object and the propagation of the errors from the hand to the last bead.

It can be seen from Fig. 8 that, comparing to the MHJ model, the MHFC one provides a better match to the experimental data consistently for all the subjects. The mean RMS errors averaged across the subjects are summarized in Table 3. For the averaged mean RMS errors, the difference between the MHJ and MHFC models is not large but systematic. For the hand trajectory, it does not exceed 0.07 cm for the position, 0.48 cm/s for the velocity, and 2.42 cm/s^2 for the acceleration. For the last bead, the corresponding differences are, respectively, 0.10 cm for the position, 0.73 cm/s for the velocity, and 5.47 cm/s^2 for the acceleration.

In addition to the RMS analysis, we compared the MHJ and MHFC models by a non-dimensional (normalized to percents) quantity, the variance accounted for (VAF). This quantity shows how much of the signal variation is accounted for by a model, disregarding possible bias of the estimates (Toth, 2010). For the *k*-th successful trial, the VAF metric is defined as

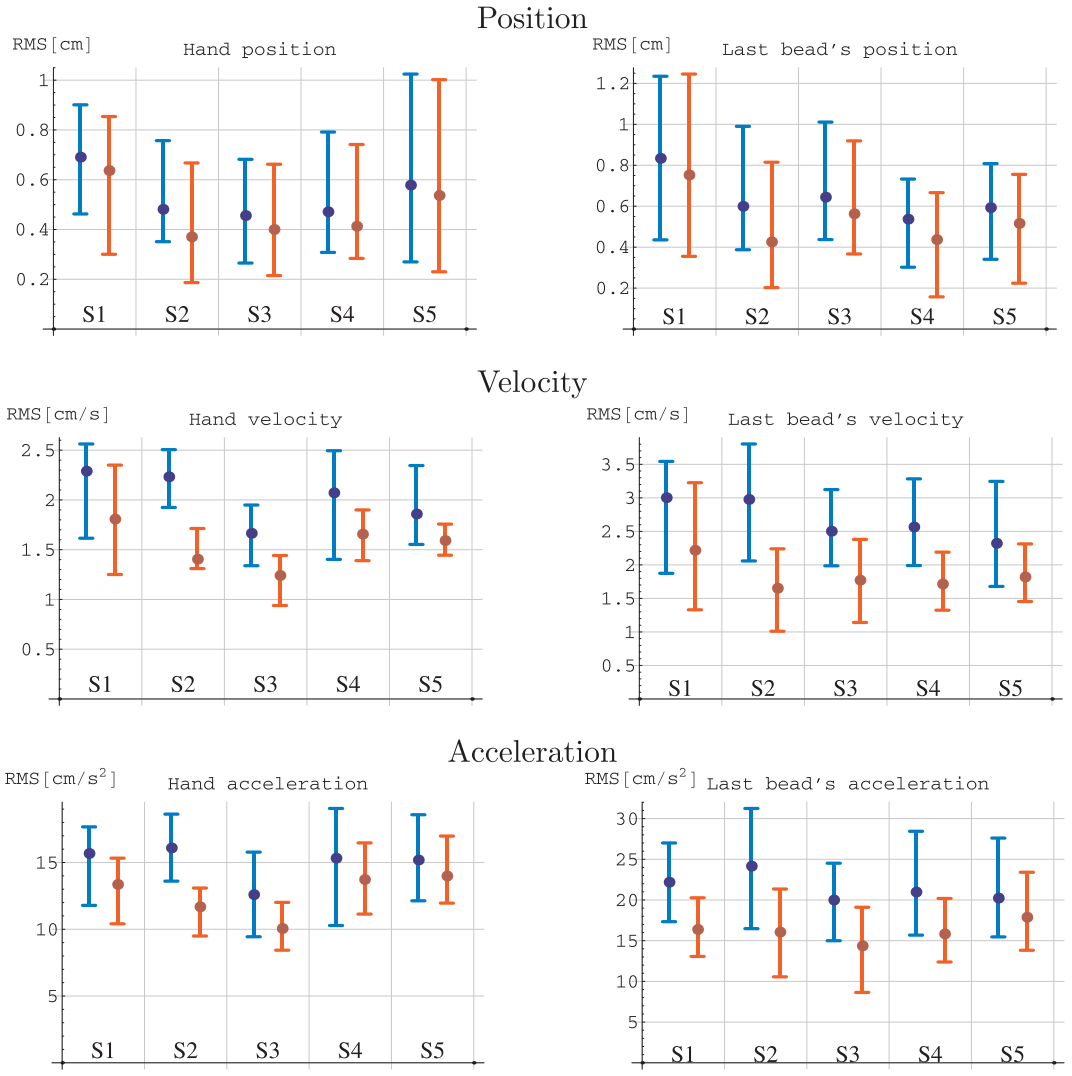

Fig. 8. RMS errors for the hand (left) and the last bead (right) trajectory profiles, predicted by the MHJ (blue), the MHFC (red) models: mean values, shown with solid points, are contoured by min–max bars. (For interpretation of the references to colour in this figure legend, the reader is referred to the web version of this article.)

Table 3
Mean RMS errors averaged across the subjects.

Model	Pos. [cm]		Vel. [cm/s]		Acc. [cm/s^2]	
	x_0	x_{10}	v_0	v_{10}	a_0	a_{10}
MHJ	0.54	0.64	2.02	2.67	14.98	21.51
MHFC	0.47	0.54	1.54	1.84	12.56	16.10

$$\mathrm{VAF}_k = 100\left(1 - \frac{\sum_{i=1}^{N}\{s_k(t_i) - s^*(t_i) - \bar{s}_k + \bar{s}^*\}^2}{\sum_{i=1}^{N}\{s_k(t_i) - \bar{s}_k\}^2}\right), \tag{40}$$

where $\bar{s}_k$ and $\bar{s}^*$ are the mean values of, respectively, $s_k(t)$ and $s^*(t)$ on the movement interval. Note that the VAF metrics were calculated for the original (non-time-scaled) samples.

The VAFs for the position, velocity, and accelerations of the hand and the last bead predicted by the MHJ and MHFC models are

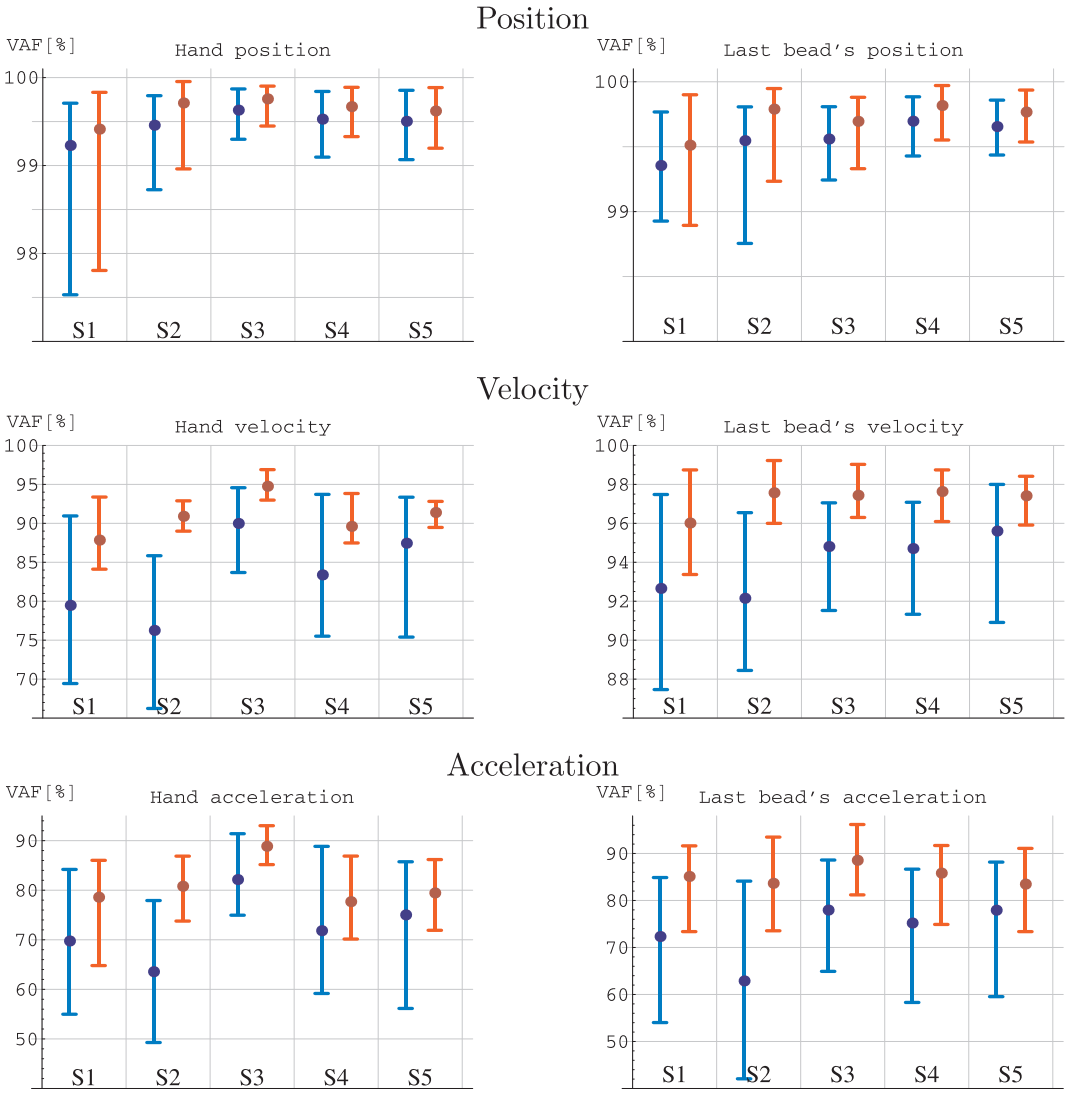

Fig. 9. VAFs for the hand (left) and the last bead (right) trajectory profiles, predicted by the MHJ (blue), the MHFC (red) models: mean values, shown with solid points, are contoured by min–max bars. (For interpretation of the references to colour in this figure legend, the reader is referred to the web version of this article.)

drawn for all subjects in the form of error bars (mean value plus/minus SD) in Fig. 9 with, respectively, blue and red colors. As expected, for the both models the position VAFs are essentially larger than the velocity ones, which in turn, are larger than the acceleration VAFs.

It is observed from Fig. 9 that again the MHFC model has a consistent edge over the MHJ one for all the subjects. The mean VAFs averaged across the subjects are summarized in Table 4. For the averaged mean VAFs, the difference between the MHJ and MHFC models increases as it goes from positions to velocities and accelerations. For the hand trajectory, it does not exceed 0.16% for the position, 7.59% for the velocity, and 8.52% for the acceleration. For the last bead, the corresponding differences are, respectively, 0.16% for the position, 3.22% for the velocity, and 12.06% for the acceleration.

Table 4
Mean VAFs [%] averaged across the subjects.

Model	Position		Velocity		Acceleration	
	x_0	x_{10}	v_0	v_{10}	a_0	a_{10}
MHJ	99.47	99.56	83.31	93.99	72.46	73.26
MHFC	99.63	99.72	90.90	97.21	81.08	85.32

It should be noted that overall the mean VAFs (averaged across the subjects) for the hand velocity and acceleration are consistently lower than those for the last bead of the flexible object. There are several reasons that may explain it. First, the experimental hand velocities and accelerations are noisier and have higher variances as they measured directly by the haptic device (velocity) or obtained by numerical differentiation (acceleration), while the bead velocities and accelerations are obtained through the real-time simulation of the object dynamics. Second, the linear springs connected in cascade act as a mechanical filter attenuating higher frequencies of the input signal and sequentially (from the first to the last) smoothing the bead velocities and accelerations. The third reason may be linked to the visual feedback. The hand position was displayed as a proxy point, not as a bead, and, comparing with the beads, it was more difficult for the subjects to trace it in performing the reaching movements.

5. Summary and discussion

An analysis of reaching movements in the manipulation of multi-mass flexible objects has been undertaken in this paper. Two theoretical approaches to modeling of reaching movements have been formulated for the cases of position and force-based actuation, resulting into four computational models. In the first approach either the position of the hand or the hand driving force is specified by an LOP satisfying boundary conditions of the reaching task. The second approach is based on the minimization of either the hand jerk or the hand driving force-change, depending on the type of actuation.

Theoretical predictions by the resulting four models for a ten-mass flexible object have been tested against experimental data obtained with the use of a virtual reality-based setup. The experimental results show that, qualitatively, all the four models capture the non-trivial motion pattern featuring a double bell-shaped profile of the hand velocity. Quantitatively, however, the optimization-based models, the MHJ and MHFC ones, provide a significantly better prediction of the human movements, with the MHFC model outperforming the MHJ one by a small margin.

The results obtained in this study demonstrate that formal generalizations of the concept of natural motion in analytical mechanics do not work well in the context of natural human movements. On the other hand, the optimization models of reaching movements, which are largely phenomenological as they cannot be derived from the first principles (Engelbrecht, 2001; Flash et al., 2003), do a better job in predicting experimental motion patterns. However, many fundamental research issues should be addressed in future studies. In what follows, we discuss some of these issues.

5.1. Kinematics vs. dynamics

Which of the optimization models, MHJ or MHFC, is more appropriate for modeling human-like reaching movements, is closely related to the fundamental question, raised in the neuroscience literature (Wolpert, Ghahramani, & Jordan, 1995; Kawato, 1996; Kawato, 1999; Flash et al., 2003), in what coordinates, kinematic or dynamic, does the CNS plan arm movements? Note that contrary to movements in free space, the two models under comparison, the kinematic and dynamic ones, take into account the dynamics of the environment represented by the flexible object.

The MHJ model implies that the CNS plans arm movements in kinematic coordinates (hand position). It is presumed that the human arm, controlled by the CNS, is an ideal actuator driving the hand in the task space. Under this assumption, the arm dynamics are already “pre-wired” in the CNS while the object dynamics (i.e., the novel environment) are acquired through learning. Thus, the trajectories of the human hand are predicted without taking into account the inertial properties of the arm. The MHFC model, on the other hand, implies that the CNS plans arm movements in dynamic coordinates (hand force). The arm dynamics are not ignored under such an assumption and must be taken into account in predicting the hand trajectories.

5.2. Task space vs. joint space

The optimization models developed in our paper are formulated in the task space. They are low parametric and admit analytical representations. However, more insight can be gained if we formulate them in the joint space of the human arm. In this connection, it would be interesting to compare our experimental data with the predictions obtained by the minimum joint torque (Uno et al., 1989) and hand force change models (Ohta, Svinin, Luo, Hosoe, & Laboissière, 2004). A further extension to the muscle level, resulting to the minimum muscle tension change model (Dornay, Uno, Kawato, & Suzuki, 1996), or even to the metabolic level, reflecting the physiological characteristics of the human arm (Kashima & Isurugi, 1998; Kashima, Isurugi, & Shima, 2000), is also possible. Note that the problem one faces in dealing with the joint and muscle level models is imprecise, if not poor, knowledge of the mass-inertia parameters of the human arm and the muscular system. Also, the joint and muscle level models are high parametric ones and, therefore, tuning the parameters in fitting of experimental data can be much more involving compared with the task space models.

5.3. Different flexible objects

Another way to discriminate between the MHJ and MHFC models is to modify the dynamic environment itself. In the context of our study, it means changing the parameters of the flexible object, its mass and stiffness. Note that the analytical structure of the solutions provided by these models, represented by combination of ordinary and trigonometric polynomials, admits, in principle, the existence of not only two-phased profiles but also those with three and more peaks. In principle, one can find a set of parameters producing two essentially different theoretical predictions, thus designing a critical test. However, one cannot ensure that the reaching movements in such a dynamic environment would be learnable in a reasonably affordable amount of time. In our opinion,

based on a limited but nevertheless practical experience, this is one of the most difficult problems in designing critical tests and the corresponding experimental setups and protocols.

The main difficulty in setting up critical tests is that the theoretical velocity profiles with sharply distinct multiple peaks appears when the product of $\omega = \sqrt{k/m}$ and the reaching time T is relatively small. In our preliminary (and not exhaustive) trials with the manipulation of very flexible objects, an extremely low success rate was registered, One may presume that an acceptable performance in reaching movements of very flexible objects would require much more skills, and the time necessary to acquire these skills can be quite large. In any case, the learnability of reaching movements in novel dynamic environments and its connection to visual and haptic feedback (Huang, Gillespie, & Kuo, 2007; Danion, Diamond, & Flanagan, 2012) remains an open issue that needs to be addressed in future research.

5.4. Alternative feedforward models

Different computational models should be tested in the future research. For the models formulated in the task space, this may include the minimum time (Happee, 1992; Hoff, 1994; Svinin, Yamamoto, & Goncharenko, 2010) and the minimum hand acceleration (Ben-Itzhak & Karniel, 2008) models. Computationally, these models are similar in that the performance index does not depend on the control and at least one more parameter—the absolute value of the maximal control signal—enters the models.

It should be noted that the extension of the minimum hand acceleration model to the minimum acceleration of the center of mass was proposed and verified for reaching movements with one bead flexible object (Leib & Karniel, 2012). We did not test this model by the following reasons. First, the values of the hand mass were estimated but not reported in (Leib & Karniel, 2012). Second, it is not truly an optimal control model as the motion of the center of mass is not derived from the necessary conditions of optimality but postulated in a polynomial form. Third, it is not extendable to different dynamic environments. There are environments (think, for example, of a block of mass held by the hand over a vertical pulley, with masses of the block and the hand being equal) where the center of mass of the hand and object system does not change at all.

Finally, the minimum variance model (Harris & Wolpert, 1998), considering human movements from the stochastic perspective, should also be given serious attention. However, as shown in (Svinin & Yamamoto, 2011), for linear control plants having at least one zero eigenvalue—and this is the case in our settings since the stiffness of the hand itself is not considered in modeling of reaching movements—this model is equivalent to either the MHJ or the MHFC model, depending on the type of actuation.

5.5. Feedforward vs. feedback control

It is well known that the feedforward optimal control can be represented in the feedback form but the control gains at the terminal point tend to infinity (Bryson & Ho, 1975). To alleviate this issue, a delayed feedback can be designed (Hoff & Arbib, 1993). Alternatively, the optimal control problem can be restructured by removing the terminal boundary conditions and adding the corresponding penalty term to the performance index.

In the latter formulation, the prediction of reaching movements is transformed to finding/tuning the correct trade-off between the accuracy and the control effort. From the biological point of view, the feedback control is undoubtedly more plausible although the biological interpretation of the gain coefficients is somewhat mediated. From the mathematical point of view, however, whether the control signal is feedback or feedforward is a matter of representation and, with the right trade-off, it should not affect essentially the resulting optimal motion patterns.

It should be noted that the optimal feedback control, based on the computational scheme developed by Todorov and Jordan (2002, 2005), was verified for reaching movements with one bead flexible object (Nagengast, Braun, & Wolpert, 2009). The control signal was transformed into the hand driving force by applying a second-order muscle-like low-pass filter (Winter, 1990). The hand mass was not estimated but set as 1kg, and the damping force did not depend on the hand velocity. However, the most critical consideration is that the hand-object model employed in (Nagengast et al., 2009) (see also supplementary material (Nagengast, Braun, & Wolpert, 2009)) was not physical. Specifically, the perceived interactive haptic force was accounted for in the object dynamics but was not in the hand dynamics. Hence, we believe that the theoretical predictions reported in (Nagengast et al., 2009) need to be reexamined.

5.6. Nonlinear underactuated objects

It should be noted that studying of reaching movements in dynamic environments is still a relatively unexplored research area, with the amount of experimental data being much less that accumulated for the free-space movements. In this connection, the use of virtual reality-based haptic simulators for studying human movements can be helpful in the design of critical tests for establishing computational models capturing features of not only the free-space but also constrained reaching movements. The haptic simulators allow for the creation of a rich variety of reconfigurable dynamic environments including not only linear flexible objects but also more complex underactuated systems.

Note that the dynamics of the multi-mass flexible object with single control input considered in this paper are linear and, from the viewpoint of control theory, differentially flat (Lévine & Nguyen, 2003; Sira-Ramírez & Agrawal, 2004). Nonlinear underactuated systems are more difficult to control. Of particular importance is the control of non-differentially flat systems. This problem is challenging, as no generic approaches for motion planning, except of optimal control, are yet available for them. In this situation, the knowledge of human-like control strategies may be useful and hopefully beneficial for the design of motion control of such nonlinear

systems.

One of the examples of non-differentially flat objects is a cart-pendulum system (Ramasamy, Wu, & Sreenath, 2014) that can serve as a model of movements with a cup of coffee. Hasson, Shen, and Sternad (2012) analyzed human performance in reaching task with a coffee cup modeled in a haptic simulator. They characterized human-like motion planning strategies in minimum time and comfortable movement scenarios in terms of energy margins. Nasseroleslami, Hasson, and Sternad (2014, 2016) extended the formulation from reaching to rhythmic movements and showed that humans selected strategies with higher predictability of interaction dynamics. Bazzi, Ebert, Hogan, and Sternad (2018) analyzed the stability of interaction dynamics with the use of contraction theory and verified that humans exploit stability to reduce sensitivity to internal noise and external perturbations. While these studies expose and demonstrate the important role of stability and predictability, the optimality of human movements in control of nonlinear objects with internal degrees of freedom remains to be analyzed and verified by computational models.

Acknowledgements

This research was supported, in part, by Ritsumeikan University (Research Promotion Program for Acquiring Grants-in-Aid for Scientific Research).

Appendix A

1º. *Clamped-free flexible object.* Consider the system (2, 3) with $x_0 = 0$. In the matrix form, it can be represented as $\boldsymbol{M}\ddot{\boldsymbol{x}} + \boldsymbol{K}\boldsymbol{x} = \boldsymbol{0}$, where $\boldsymbol{x} = (x_1, x_2, ..., x_n)^{\mathrm{T}}$, $\boldsymbol{M} = m\boldsymbol{I}$ is the mass matrix, $\boldsymbol{I}$ is the $n \times n$ identify matrix, and

$$\boldsymbol{K} = k\begin{bmatrix} 2 & -1 & 0 & \dots & 0 & 0 & 0 \\ -1 & 2 & -1 & \dots & 0 & 0 & 0 \\ \vdots & \vdots & \vdots & \ddots & \vdots & \vdots & \vdots \\ 0 & 0 & 0 & \dots & -1 & 2 & -1 \\ 0 & 0 & 0 & \dots & 0 & -1 & 1 \end{bmatrix} \triangleq k\overline{\boldsymbol{K}}, \tag{41}$$

is the stiffness matrix. As this system is conservative, the eigenvalues, defined by $\det(\boldsymbol{M}\lambda^2 + \boldsymbol{K}) = 0$, are purely imaginary (Meirovitch, 1967): $\lambda_k = \pm ip_k$, where p_k, $k = 1, ..., n$, are the natural frequencies of the clamped-free flexible object. Replace λ^2 by $-p^2$. Then from $\det(k\overline{\boldsymbol{K}} - m\boldsymbol{I}p^2) = 0$ one obtains $\det(\overline{\boldsymbol{K}} - \nu\boldsymbol{I}) = 0$, where $\nu = p^2/\omega^2$ is the eigenvalue of matrix $\overline{\boldsymbol{K}}$.

The characteristic equation, $\det(\overline{\boldsymbol{K}} - \nu\boldsymbol{I}) = 0$, can be written down as $D_n = 0$, where

$$D_n = \begin{vmatrix} 2-\nu & -1 & 0 & \dots & 0 & 0 & 0 \\ -1 & 2-\nu & -1 & \dots & 0 & 0 & 0 \\ \vdots & \vdots & \vdots & \ddots & \vdots & \vdots & \vdots \\ 0 & 0 & 0 & \dots & -1 & 2-\nu & -1 \\ 0 & 0 & 0 & \dots & 0 & -1 & 1-\nu \end{vmatrix} \tag{42}$$

is the characteristic determinant. It can be unfolded by the following recurrence relations

$$D_i = (2-\nu)D_{i-1} - D_{i-2}, \quad i = 2, ..., n, \tag{43}$$

with initial conditions

$$D_1 = (1-\nu), \quad D_0 = 1. \tag{44}$$

Using these relations and the principle of mathematical induction, it is easy to prove that

$$D_n = \sum_{s=0}^{n} \frac{C_{n+s}^{n-s}}{\omega^{2s}}\lambda^{2s}, \tag{45}$$

from which it follows that $D_n = 0$ is a part of Eqs. (19) and (30).

For $\nu = 2(1-x)$ the characteristic determinants turn into the Chebyshev polynomials of the 3rd kind: $D_0 = 1$, $D_1 = 2x - 1$, $D_i = 2xD_{i-1} - D_{i-2}$, $i = 2, ..., n$. By setting $x = \cos\theta$, one represents the Chebyshev polynomials as (Mason & Handscomb, 2003):

$$D_i = \frac{\cos\left((i+\frac{1}{2})\theta\right)}{\cos\frac{1}{2}\theta}, \quad i = 1, 2, ..., n. \tag{46}$$

By solving $D_n = 0$, one defines

$$\theta_i = \frac{2i-1}{2n+1}\pi, \quad i = 1, 2, ..., n, \tag{47}$$

and obtains the natural frequencies of the clamped-free flexible object

$$p_i = 2\omega\sin\left(\frac{\theta_i}{2}\right), \quad i = 1, 2, ..., n. \tag{48}$$

2°. *Flexible object with free ends.* Consider now the system (1, 2,3) with $f = 0$ In the matrix form it can be represented as $\boldsymbol{M}\ddot{\boldsymbol{x}} + \boldsymbol{K}\boldsymbol{x} = \boldsymbol{0}$, where the vector $\boldsymbol{x} = (x_0, x_1, x_2, ..., x_n)^{\mathrm{T}}$, $\boldsymbol{M} = \mathrm{diag}\{m_0, m, ..., m\}$ is the mass matrix, and

$$\boldsymbol{K} = k\begin{bmatrix} 1 & -1 & 0 & 0 & ... & 0 & 0 & 0 \\ -1 & 2 & -1 & 0 & ... & 0 & 0 & 0 \\ 0 & -1 & 2 & -1 & ... & 0 & 0 & 0 \\ \vdots & \vdots & \vdots & \vdots & \ddots & \vdots & \vdots & \vdots \\ 0 & 0 & 0 & 0 & ... & -1 & 2 & -1 \\ 0 & 0 & 0 & 0 & ... & 0 & -1 & 1 \end{bmatrix}, \tag{49}$$

is the stiffness matrix. The characteristic equation for this system can be written down as $D_{n+1} = 0$, where

$$D_{n+1} = \begin{vmatrix} \mu - \nu & -\mu & 0 & 0 & ... & 0 & 0 & 0 \\ -1 & 2 - \nu & -1 & 0 & ... & 0 & 0 & 0 \\ 0 & -1 & 2 - \nu & -1 & ... & 0 & 0 & 0 \\ \vdots & \vdots & \vdots & \vdots & \ddots & \vdots & \vdots & \vdots \\ 0 & 0 & 0 & 0 & ... & -1 & 2 - \nu & -1 \\ 0 & 0 & 0 & 0 & ... & 0 & -1 & 1 - \nu \end{vmatrix}, \tag{50}$$

and the mass ratio $\mu = m/m_0$. The characteristic determinant is calculated as $D_{n+1} = (\mu - \nu)D_n - \mu D_{n-1}$, where D_n and D_{n-1} are defined recursively from (43) and (44) or, by replacing ν to θ, from (46) for $i = n$ and $i = n - 1$, respectively. Using these relations and the principle of mathematical induction, one can prove that

$$D_{n+1} = \sum_{s=0}^{n} \frac{C_{n+s}^{n-s}}{\omega^{2s}} \left\{ \lambda^{2s+2} + \frac{2s\mu\omega^2}{n+s}\lambda^{2s} \right\}, \tag{51}$$

from which it follows that for $\lambda \neq 0$, $D_{n+1} = 0$ is a part of equations (23) and (36).

In terms of θ, the condition $D_{n+1} = 0$ can be represented now as

$$2\sin\frac{\theta}{2}\{\tan n\theta(\mu - 1 + \cos\theta) + \sin\theta\} = 0. \tag{52}$$

This equation has one zero root corresponding to the rigid body mode, and n non-zero roots $\widetilde{\theta}_i$, $i = 1, ..., n$, that are found numerically by solving

$$\mu = 1 - \cos\theta - \sin\theta\cot n\theta \tag{53}$$

for a given mass ratio μ. The natural frequencies of the free-free flexible object are then established as

$$\widetilde{p}_i = 2\omega\sin\left(\frac{\widetilde{\theta}_i}{2}\right), \quad i = 1, 2, ..., n. \tag{54}$$

Appendix B

1°. *Kinematic LOP model.* By differentiating (20) $2l$ times and substituting the result into (7), one obtains

$$x_0(t) = \sum_{l=0}^{n} \sum_{i=2l}^{2n+5} \alpha_i \frac{C_{n+l}^{n-l} C_i^{2l} (2l)!}{\omega^{2l}} t^{i-2l} + \sum_{i=1}^{n} \sum_{l=0}^{n} \frac{C_{n+l}^{n-l}}{\omega^{2l}} (-1)^l p_i^{2l} \beta_i \sin\left(p_i t + \gamma_i\right). \tag{55}$$

The last double sum in (55) vanishes because

$$\sum_{l=0}^{n} \frac{C_{n+l}^{n-l}}{\omega^{2l}} (-1)^l p_i^{2l} = 0, \tag{56}$$

which follows from the characteristic equation for the differential Eq. (7) with $\lambda_i = \pm\imath p_i$. Thus, the structure of $x_0(t)$ has a pure polynomial form.

2°. *MHJ model.* By differentiating (31) $2l$ times and substituting the result into (7), one obtains

$$x_0(t) = \sum_{l=0}^{n} \sum_{i=2l}^{5} \alpha_i \frac{C_{n+l}^{n-l} C_i^{2l} (2l)!}{\omega^{2l}} t^{i-2l} + \sum_{i=1}^{n} \sum_{l=0}^{n} \frac{C_{n+l}^{n-l}}{\omega^{2l}} (-1)^{l+1} 2l p_i^{2l-1} \delta_i \cos\left(p_i t + \varepsilon_i\right) + \sum_{i=1}^{n} \sum_{l=0}^{n} \frac{C_{n+l}^{n-l}}{\omega^{2l}} (-1)^l p_i^{2l} \left\{ \beta_i \sin\left(p_i t + \gamma_i\right) + t\,\delta_i \sin\left(p_i t + \varepsilon_i\right) \right\}. \tag{57}$$

The last double sum in (57) vanishes by virtue of (56). Thus, the structure of $x_0(t)$ has the form (32).

Appendix C

In analytical mechanics, a system is called natural if it admits a potential function $V(\boldsymbol{q}, \dot{\boldsymbol{q}})$ (Gantmacher, 1975; Arnold, 1980), where $\boldsymbol{q} \in \mathbb{R}^n$ is the vector of generalized coordinates. Natural systems satisfy the variational Hamilton principle $\delta \int_0^T L(\boldsymbol{q}, \dot{\boldsymbol{q}}) \mathrm{d}t = 0$, where $L = K - V$, and K is the kinetic energy. For the natural systems, Lagrange's equations of motion have the form: $\frac{\mathrm{d}}{\mathrm{d}t}\left(\frac{\partial L}{\partial \dot{\boldsymbol{q}}}\right) - \frac{\partial L}{\partial \boldsymbol{q}} = 0$. If there are non-conservative forces, there takes place the extended Hamilton principle $\int_0^T (\delta L - \delta W) \mathrm{d}t = 0$, where $\delta W = \delta \boldsymbol{q}^{\mathrm{T}} \boldsymbol{u}$ is the virtual work of the non-conservative forces $\boldsymbol{u}$. The motion equations are then set in the familiar form:

$$\frac{\mathrm{d}}{\mathrm{d}t}\left(\frac{\partial L}{\partial \dot{\boldsymbol{q}}}\right) - \frac{\partial L}{\partial \boldsymbol{q}} = \boldsymbol{u}. \tag{58}$$

Note that the extended Hamilton principle is not variational because one cannot set δ in front of the integral. Also note that this principle is only a tool for the derivation of motion equations. It does not say anything about the solution as it obviously depends on the specific control $\boldsymbol{u}$. Nevertheless, this principle and the related concept of natural systems can be used to formally define natural reaching movements (Morita & Ohtsuka, 2006; Morita, 2012). The definition is based on the introduction of the coordinate transformation $\boldsymbol{\varphi}^{(k)} = \boldsymbol{q}$. This is a differential transformation of the original coordinates $\boldsymbol{q}$ to the new coordinates $\boldsymbol{\varphi}$. Therefore, it brings new integration constants that have to be selected in order to satisfy the boundary conditions of the reaching task:

$$\boldsymbol{q}(0) = \boldsymbol{q}_0,\ \dot{\boldsymbol{q}}(0) = \dot{\boldsymbol{q}}_0,\ \ddot{\boldsymbol{q}}(0) = \ddot{\boldsymbol{q}}_0,\ \ldots,\ \boldsymbol{q}^{(l)}(0) = \boldsymbol{q}_0^{(l)}, \tag{59}$$

$$\boldsymbol{q}(T) = \boldsymbol{q}_T,\ \dot{\boldsymbol{q}}(T) = \dot{\boldsymbol{q}}_T,\ \ddot{\boldsymbol{q}}(T) = \ddot{\boldsymbol{q}}_T,\ \ldots,\ \boldsymbol{q}^{(l)}(T) = \boldsymbol{q}_T^{(l)}. \tag{60}$$

In the new coordinates $\boldsymbol{\varphi}$, the Hamilton principle takes the following form: $\delta \int_0^T L(\boldsymbol{\varphi}^{(k)}, \boldsymbol{\varphi}^{(k+1)}) \mathrm{d}t = 0$. As shown in (Morita & Ohtsuka, 2006; Morita, 2012), in the new coordinates $\boldsymbol{\varphi}$ the system becomes natural if one sets

$$\boldsymbol{u}^{(k)} = \boldsymbol{0}. \tag{61}$$

By this definition the control force $\boldsymbol{u}$ becomes conservative with respect to the new coordinates $\boldsymbol{\varphi}$, while it is non-conservative with respect to the original coordinates $\boldsymbol{q}$ (Morita & Ohtsuka, 2006; Morita, 2012).

The solution of (61) defines the control $\boldsymbol{u}$ in the LOP form. Given the number l in (59, 60), the order k of the polynomial is established as follows. The differential Eq. (61) has nk integration constants. The number of boundary conditions in (59, 60) is $2n(l+1)$, and motion Eqs. (58) presume $2n$ integration constants. The numbers of integration constants are balanced if $nk = 2n(l+1) - 2n$, which gives $k = 2l$. Having established k, the trajectory of the natural reaching movement is defined by solving motion Eqs. (58) with the control force (61) under the boundary conditions (59, 60).

As confirmed in (Morita & Ohtsuka, 2006; Morita, 2012), this method allows for capturing the invariant features of reaching movements in the free space (a rough straightness of the hand path and the bell-shaped hand velocity profile). It is also interesting to note that the LOP form of the control input results from the extension of yet another general principle of analytical mechanics—the Gauss principle of least constraints—to the control of mechanical systems (Soltakhanov et al., 2009; Zegzhda et al., 2016).

Appendix D

Typically, in the estimation of the hand mass the human hand is modeled as a mass-damper-spring system, and this model holds for small movements and a short period of time. Based on this model, the hand impedance can be evaluated by perturbing, for example by a robotic manipulandum, the hand during maintenance of a given posture and measuring the hand displacement. This perturbation technique is reported in (Tsuji, Morasso, Goto, & Ito, 1995; Speich, Shao, & Goldfarb, 2005; Itkowitz, Handley, & Zhu, 2006) However, its use for a light weight haptic device without additional hardware, such as the one proposed in (Fu & Çavuşoğlu, 2012), can be problematic.

A simple method, based on the accommodation to forced vibrations and applicable to the estimation of the hand mass only, can be constructed as follows. Assume that a human subject can follow the motion of a virtual object of mass m_1, connected to the hand by a

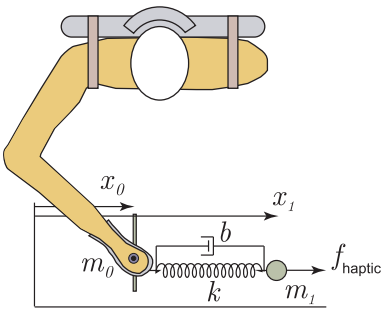

Fig. 10. Hand mass estimation by following a haptic force.

spring of stiffness k and a damper of viscosity b, without developing his or her own driving force as sketched in Fig. 10. Assume also that a periodic force of amplitude F and frequency Ω is applied to the hand, and the total haptic force is defined as

$$f_{\text{haptic}} = b(\dot{x}_1 - \dot{x}_0) + k(x_1 - x_0) + F\cos\Omega t. \tag{62}$$

The dynamics of the composite system (the hand and the virtual object) are described as

$$m_0\ddot{x}_0 + b(\dot{x}_0 - \dot{x}_1) + k(x_0 - x_1) = F\cos\Omega t, \tag{63}$$

$$m_1\ddot{x}_1 + b(\dot{x}_1 - \dot{x}_0) + k(x_1 - x_0) = 0. \tag{64}$$

The motion of the center of mass, $x_{\text{cm}} = (m_0x_0 + m_1x_1)/(m_0 + m_1)$, is governed by $(m_0 + m_1)\ddot{x}_{\text{cm}} = F\cos\Omega t$ and, under the zero initial conditions, one obtains

$$x_{\text{cm}}(t) = \frac{F}{(m_0 + m_1)\Omega^2}(1 - \cos\Omega t). \tag{65}$$

Upon resolving for x_1 (with respect to x_0 and x_{cm}) and x_0 (with respect to x_1 and x_{cm}), the system dynamics are decoupled as

$$\ddot{x}_0 + 2n\dot{x}_0 + \omega^2x_0 = 2n\dot{x}_{\text{cm}} + \omega^2x_{\text{cm}} + \frac{F}{m_0}\cos\Omega t, \tag{66}$$

$$\ddot{x}_1 + 2n\dot{x}_1 + \omega^2x_1 = 2n\dot{x}_{\text{cm}} + \omega^2x_{\text{cm}}, \tag{67}$$

where

$$\omega = \sqrt{\frac{k(m_0 + m_1)}{m_0m_1}}, \quad n = \frac{b(m_0 + m_1)}{2m_0m_1} \tag{68}$$

are, respectively, the natural frequency and the damping factor.

It can be shown that, for the low resistance case ($n < \omega$), the steady state solution to the system dynamics is developed as

$$\hat{x}_0(t) = \frac{F}{(m_0 + m_1)\Omega^2}(1 - a\cos(\Omega t + \alpha)), \tag{69}$$

$$\hat{x}_1(t) = \frac{F}{(m_0 + m_1)\Omega^2}(1 - b\cos(\Omega t + \beta)), \tag{70}$$

where

$$a = \sqrt{\frac{\{\omega^2 - (1 + \mu)\Omega^2\}^2 + 4n^2\Omega^2}{(\omega^2 - \Omega^2)^2 + 4n^2\Omega^2}}, \tag{71}$$

$$b = \sqrt{\frac{\omega^4 + 4n^2\Omega^2}{(\omega^2 - \Omega^2)^2 + 4n^2\Omega^2}}, \tag{72}$$

$$\tan\alpha = \frac{2n\mu\Omega^3}{(\omega^2 - \Omega^2)\{\omega^2 - (1 + \mu)\Omega^2\} + 4n^2\Omega^2}, \tag{73}$$

$$\tan\beta = -\frac{2n\Omega^3}{\omega^2(\omega^2 - \Omega^2) + 4n^2\Omega^2}, \tag{74}$$

and $\mu = m_1/m_0$.

By measuring the differences of the peak amplitudes for the hand and/or the object, Δx_0, Δx_1, one can estimate the hand mass from one of the following nonlinear (with respect to m_0) relationships:

$$\Delta x_0 = \frac{2Fa}{(m_0 + m_1)\Omega^2}, \quad \Delta x_1 = \frac{2Fb}{(m_0 + m_1)\Omega^2}. \tag{75}$$

Note that for a relatively large natural frequency $\omega^2 \gg \Omega^2$ and a sufficiently small damping factor n, we have $a \approx 1$, $b \approx 1$, and the estimation equations become linear and therefore easier to use. Either of them can be used for the estimation of the hand mass m_0. Practically, however, it is more preferable to deal with the second one as the measurement of Δx_1 is less noisy because (64) acts as a second order low-pass filter.

In our experiments, the parameters of the haptic simulator were set as follows: $m_1 = 1$ kg, $F = 1.8$ N, $\Omega = \pi$ rad/s, $k = 600N$/m, $b = 0.05$ Ns/m. The haptic force along the movement line was computed by (62), while that in the lateral directions was modeled by a virtual spring of stiffness 600 N/m. The object dynamics (64) were simulated in the computer (the 4th-order Runge–Kutta method with constant step 0.001 s). The subjects were requested to hold the PHANToM stylus at the configuration similar to the one they had used in the production of reaching movements in the previously completed experiments. The subjects were instructed not to resist the motion of the virtual object and follow it in the most comfortable mode, without exerting his own driving force or minimizing it as much as possible.

Table 5
Effective hand masses m_0 [kg].

Subject	Avg.	Min.	Max.	SD
S1	0.362	0.108	0.805	0.156
S2	0.397	0.162	0.693	0.131
S3	0.461	0.242	0.730	0.108
S4	0.412	0.127	0.911	0.174
S5	0.503	0.201	0.882	0.149

The positions of the hand (a proxy point) and the object were displayed on the computer monitor. In addition to this standard visual feedback, a digital oscillograph was implemented in a pop-up window. Two signals were displayed on the digital oscillograph, the simulated object position and the reference signal (70), computed initially with $m_0 = 1$ kg, and the simulated object position. The subjects were instructed to synchronize frequencies of these two signals. They could also incrementally adjust the amplitude of the reference signal (the reference value of m_0) by pressing up and down arrow buttons on the computer keyboard.

Each subject underwent 20 trials, and each trial lasted, on average, 3 min. The samples of the differences of the peak amplitudes Δx_1 at the synchronized fragments of the reference and simulated signals were collected for analysis. The number of samples in each trial exceeds 50. The average, minimum, and maximum estimates of the hand mass as well as the SD from the averages are listed in Table 5.

It should be noted that the estimated average values of the hand mass are slightly higher than those reported in (Fu & Çavuşoğlu, 2012) for motion along the x-axis. However, the variability of the hand mass, stipulated by slight changes of the arm configuration and the grip force in different trials, is compatible with (Fu & Çavuşoğlu, 2012).

References

Abend, W., Bizzi, E., & Morasso, P. (1982). Human arm trajectory formation. *Brain, 105*, 331–348.

Amirabdollahian, F., Loureiro, R., & Harwin, W. (2002). Minimum jerk trajectory control for rehabilitation and haptic applications. *Proc. IEEE International Conference on Robotics and Automation. Washington D.C.* (pp. 3380–3385). .

Arimoto, S., Sekimoto, M., Hashiguchi, H., & Ozawa, R. (2005). Natural resolution of ill-posedness of inverse kinematics for redundant robots: A challenge to Bernstein's degrees-of-freedom problem. *Advanced Robotics, 19*(4), 401–434.

Arnold, V. (1980). *Mathematical Methods of Classical Mechanics.* Berlin: Springer-Ferlag.

Aspinwall, D. (1990). Acceleration profiles for minimizing residual response. *ASME Journal of Dynamic Systems, Measurement, and Control, 102*(1), 3–6.

Atkeson, C., & Hollerbach, J. (1985). Kinematic features of unrestrained vertical arm movements. *Journal of Neuroscience, 5*(9), 2318–2330.

Bazzi, S., Ebert, J., Hogan, N., & Sternad, D. (2018). Stability and predictability in human control of complex objects. Chaos: An Interdisciplinary. *Journal of Nonlinear Science, 28*(10), 103103 .

Ben-Itzhak, S., & Karniel, A. (2008). Minimum acceleration criterion with constraints implies bang-bang control as an underlying principle for optimal trajectories of arm reaching movements. *Neural Computation, 20*(3), 779–812.

Bernstein, N. (1967). *The coordination and regulation of movements.* London: Pergamon.

Bryson, A., & Ho, Y.-C. (1975). *Applied optimal control: Optimization, Estimation and Control.* New York: Hemisphere Publishing Corporation.

Çavuşoğlu, M., Feygin, D., & Tendick, F. (2002). A critical study of the mechanical and electrical properties of the PHANToM haptic interface and improvements for high performance control. *Presence: Teleoperators and Virtual Environments, 11*(6), 555–568.

Chan, T., Stelson, K. (1995). Point-to-point motion commands that eliminate residual vibration. In: Proc. American Control Conference. vol. 1. Seattle, Washington, pp. 909–913.

Danion, F., Diamond, J., & Flanagan, J. (2012). The role of haptic feedback when manipulating nonrigid objects. *Journal of Neurophysiology, 107*(1), 433–441.

Dingwell, J., Mah, C., & Mussa-Ivaldi, F. (2004). Experimentally confirmed mathematical model for human control of a non-rigid object. *Journal of Neurophysiology, 91*, 1158–1170.

Dornay, M., Uno, Y., Kawato, M., & Suzuki, R. (1996). Minimum muscle-tension-change trajectories predicted by using a 17-muscle model of the monkey's arm. *Journal of Motor Behavior, 28*, 83–100.

Engelbrecht, S. (2001). Minimum principles in motor control. *Journal of Mathematical Psychology, 45*, 497–542.

Flash, T., & Hogan, N. (1985). The coordination of arm movements: An experimentally confirmed mathematical model. *The Journal of Neuroscience, 5*(7), 1688–1703.

Flash, T., Hogan, N., & Richardson, M. (2003). Optimization principles in motor control. In M. Arbib (Ed.). *The handbook of brain theory and neural networks* (pp. 827–831). (2nd ed.). Cambridge, Massachusetts: MIT Press.

Fu, M., & Çavuşoğlu, M. (2012). Human-arm-and-hand-dynamic model with variability analyses for a stylus-based haptic interface. *IEEE Transactions on Systems, Man, and Cybernetics, Part B (Cybernetics), 42*(6), 1633–1644.

Gantmacher, F. (1975). *Lectures in analytical mechanics.* Moscow: Mir Publishers.

Happee, R. (1992). Time optimality in the control of human movements. *Biological Cybernetics, 66*(4), 357–366.

Harris, C., & Wolpert, D. (1998). Signal-dependent noise determines motor planning. *Nature, 394*, 780–784.

Hasson, C., Shen, T., & Sternad, D. (2012). Energy margins in dynamic object manipulation. *Journal of Neurophysiology, 108*(5), 1349–1365.

Hoff, B. (1994). A model of duration in normal and perturbed reaching movement. *Biological Cybernetics, 71*(6), 481–488.

Hoff, B., & Arbib, M. (1993). Models of trajectory formation and temporal interaction of reach and grasp. *Journal of Motor Behavior, 25*, 175–192.

Huang, F., Gillespie, R., & Kuo, A. (2007). Visual and haptic feedback contribute to tuning and online control during object manipulation. *Journal of Motor Behavior, 39*(3), 179–193.

Garvin, G., Žefran, M., Henis, E., & Kumar, V. (1997). Two arm trajectory planning in a manipulation task. *Biological Cybernetics, 76*(1), 53–62.

Itkowitz, B., Handley, J., & Zhu, W. (2005). The OpenHaptics toolkit: A library for adding 3D touch navigation and haptics to graphics applications. *Eurohaptics Conference and Symposium on Haptic Interfaces for Virtual Environments and Teleoperator Systems* (pp. 590–591). Italy: Pisa.

Karnopp, B., Fisher, F., & Yoon, B. (1992). A strategy for moving a mass from one point to another. *Journal of the Frankline Institute, 329*(5), 881–892.

Kashima, T., & Isurugi, Y. (1998). Trajectory formation based on physiological characteristics of skeletal muscles. *Biological Cybernetics, 78*, 413–422.

Kashima, T., Isurugi, Y., & Shima, M. (2000). Analysis of a muscular control system in human movements. *Biological Cybernetics, 82*, 123–131.

Kawato, M. (1996). Trajectory formation in arm movements: Minimization principles and procedures. In H. Zelaznik (Ed.). *Advances in Motor Learning and Control* (pp. 225–259). Illinois: Human Kinetics Publishers.

Kawato, M. (1999). Internal models for motor control and trajectory planning. *Current Opinion in Neurobiology, 9*, 718–727.
Lacquaniti, F., Terzuolo, C., & Viviani, P. (1983). The law relating kinematic and figural aspects of drawing movements. *Acta Psychologica, 54*(1), 115–130.
Leib, R., & Karniel, A. (2012). Minimum acceleration with constraints of center of mass: A unified model for arm movements and object manipulation. *Journal of Neurophysiology, 108*(6), 1646–1655.
Lévine, J., & Nguyen, D. (2003). Flat output characterization for linear systems using polynomial matrices. *Systems & Control Letters, 48*(1), 69–75.
Itkowitz, B., Handley, J., Zhu, W. (2005). The OpenHaptics toolkit: A library for adding 3D touch navigation and haptics to graphics applications. In: Eurohaptics Conference and Symposium on Haptic Interfaces for Virtual Environments and Teleoperator Systems. Pisa, Italy, pp. 590–591.
Mason, J., & Handscomb, D. (2003). *Chebyshev Polynomials.* Boca Raton: Chapman & Hall/ CRC Press.
Maurice, P., Huber, M., Hogan, N., & Sternad, D. (2018). Velocity-curvature patterns limit human-robot physical interaction. *IEEE Robotics and Automation Letters, 3*(1), 249–256.
Meckl, P., & Kinceler, R. (1994). Robust motion control of flexible systems using feedforward forcing functions. *IEEE Transactions on Control Systems Technology, 2*(3), 245–254.
Meirovitch, L. (1967). *Analytical methods in vibrations.* New York: MacMillan Publishing Company.
Morasso, P. (1981). Spatial control of arm movements. *Experimental Brain Research, 42*(2), 223–227.
Morita, S. (2012). Trajectory generation between two arbitrary states based on Hamilton's principle: A variable substitution method. *International Journal of Humanoid Robotics, 9*(3), 1250023.
Morita, S., & Ohtsuka, T. (2006). Natural motion trajectory generation based on Hamilton's principle. *Transactions of the Society of Instrument and Control Engineers, 42*(1), 1–10 (in Japanese).
Nagengast, A., Braun, D., & Wolpert, D. (2009). Optimal control predicts human performance on objects with internal degrees of freedom. *PLoS Computational Biology, 5*(6), 1–15.
Nagengast, A., Braun, D., & Wolpert, D. (2009). Supplementary material – optimal control predicts human performance on objects with internal degrees of freedom. *PLoS Computational Biology, 5*(6), 1–23.
Nasseroleslami, B., Hasson, C., & Sternad, D. (2014). Rhythmic manipulation of objects with complex dynamics: Predictability over chaos. *PLoS Computational Biology, 10*(10), e1003900 .
Newell, A., & Rosenbloom, P. (1981). Mechanisms of skill acquisition and the law of practice. In J. Anderson (Ed.). *Cognitive Skills and Their Acquisition* (pp. 1–55). Hillsdale, NJ: Erlbaum.
Ohta, K., Svinin, M., Luo, Z., Hosoe, S., & Laboissière, R. (2004). Optimal trajectory formation of constrained human arm reaching movements. *Biological Cybernetics, 91*(1), 23–36.
Piazzi, A., & Visioli, A. (2000). Minimum-time system-inversion-based motion planning for residual vibration reduction. *IEEE/ASME Transactions on Mechatronics, 5*(1), 12–22.
Plamondon, R., Alimi, A. M., Yergeau, P., & Leclere, F. (1993). Modeling velocity profiles of rapid movements: A comparative study. *Biological Cybernetics, 69*, 119–128.
Pollick, F., Hale, J., & Tzoneva-Hadjigeorgieva, M. (2005). Perception of humanoid movements. *International Journal of Humanoid Robotics, 2*(3), 277–300.
Ramasamy, S., Wu, G., & Sreenath, K. (2014). Dynamically feasible motion planning through partial differential flatness. In D. Fox, L. Kavraki, & H. Kurniawati (Eds.). *Robotics: Science and Systems X, Berkeley*. USA: CA.
Singer, N., & Seering, W. (1990). Preshaping command inputs to reduce system vibration. *ASME Journal of Dynamic Systems, Measurement, and Control, 112*(1), 76–82.
Sira-Ramírez, H., & Agrawal, S. (2004). Differentially Flat Systems. *vol. 17 of Control Engineering*. New York: Marcel Dekker Inc.
Smith, O. (1957). Posicast control of damped oscillatory systems. *Proceedings of the IRE, 45*(9), 1249–1255.
Smith, S. (2002). *Digital signal processing: A practical guide for engineers and scientists.* Boston: Newness.
Soltakhanov, S., Yushkov, M., & Zeghda, S. (2009). *Mechanics of nonholonomic systems: A new class of control systems, foundations of engineering mechanics.* Berlin: Springer-Verlag.
Speich, J., Shao, L., & Goldfarb, M. (2005). Modeling the human hand as it interacts with a telemanipulation system. *Mechatronics, 15*, 1127–1142.
Sternad, D., & Hasson, C. (2016). Predictability and robustness in the manipulation of dynamically complex objects. In J. Laczko, & M. Latash (Vol. Eds.), *Advances in experimental medicine and biology: . vol. 957. Progress in motor control: Theories and translations* (pp. 55–77). Switzerland: Springer.
Svinin, M., Goncharenko, I., Luo, Z., & Hosoe, S. (2006). Reaching movements in dynamic environments: How do we move flexible objects? *IEEE Transactions on Robotics, 22*(4), 724–739.
Svinin, M., Yamamoto, M., Goncharenko, I. (2010). Simple models in trajectory planning of human-like reaching movements. In: Proc. IEEE/RSJ Int. Conference on Intelligent Robots and Systems, IROS'2010. Taipei, Taiwan, vol. 1, pp. 1662–1667.
Svinin, M., Yamamoto, M. (2011). A mathematical analysis of the minimum variance model of human-like reaching movements. In: Proc. IEEE/RSJ Int. Conference on Intelligent Robots and Systems, IROS'2011. San Francisco, CA, vol. 4, pp. 4368–4391.
Todorov, E. (2005). Stochastic optimal control and estimation methods adapted to the noise characteristics of the sensorimotor system. *Neural Computation, 17*(5), 1084–1108.
Todorov, E., & Jordan, M. (2002). Optimal feedback control as a theory of motor coordination. *Nature Neuroscience, 5*, 1226–1235.
Toth, R. (2010). Modeling and identification of linear parameter-varying systems. *Vol. 403 of lecture notes in control and information sciences*. Berlin Heidelberg: Springer-Verlag.
Tsuji, T., Morasso, P., Goto, K., & Ito, K. (1995). Human hand impedance characteristics during maintained posture in multi-joint arm movements. *Biological Cybernetics, 72*, 475–485.
Tsuji, T., Tanaka, Y., Morasso, P., Sanguineti, V., & Kaneko, M. (2002). Bio-mimetic trajectory generation of robots via artificial potential field with time base generator. *IEEE Transactions on Systems, Man, and Cybernetics—Part C: Applications and Reviews, 32*(4), 426–439.
Uno, Y., Kawato, M., & Suzuki, R. (1989). Formation and control of optimal trajectory in human multijoint arm movement. Minimum torque-change model. *Biological Cybernetics, 61*, 89–101.
Winter, D. (1990). *Biomechanics and motor control of human movement.* New York: John Wiley and Sons.
Wolpert, D., Ghahramani, Z., & Jordan, M. (1995). Are arm trajectories planned in kinematic or dynamic coordinate? An adaptation study. *Experimental Brain Research, 103*, 460–470.
Zegzhda, S., Shatrov, E., Yushkov, M. (2016). A new approach to finding the control transporting a system from one phase state to another. Vestnik of Saint Petersburg University, Series 1: Mathematics, Mechanics, Astronomy 61 (2), 284–292 (In Russian).